Table 3
Gene networks and their primary functions after DEN and ENU treatment.

Networks	Molecules in network	Top functions
(A) DEN 4 h		
1	Adaptor protein 2, Ahr-aryl hydrocarbon-*Arnt*, *Arf*, ***Bax***, ***Btg2***, *Casp1*, Caspase, *Cbp/p300*, ***Ccng1***, ***Cdkn1a***, *Creb*, Cyclin A, Cyclin E, *E2f*, *Erk1/2*, *Gadd45*, ***Gadd45b***, *Gadd45g*, ***Gdf15***, *Gsk3*, *Hist1h1c*, ***Hspb1***, ***Hspb2***, *Jun/Junb/Jund*, ***Mdm2***, *Mek1/2*, *Pak*, *Pdgf*, ***Plk2***, *Pml*, ***Pmm1***, *Pp2a*, *Rb*, *Stat*, *Trp53*	Cancer, Cell cycle, reproductive system disease
2	*Aatf*, *Aldh3a1*, *App*, beta-estradiol, *Ccne2*, ***Ccng2***, ***Cyp1a2***, ***Cpy21a1***, ***Cyp4a10***, *E2F1*, *Fabp5*, ***Gdf15***, *Gyk*, ***Glul***, *Hprt1*, *Hspa1b*, ***Igfbp1***, *Igfbp7*, *Il10*, *Il1b*, *Irf2*, *Klf10*, *MAZ*, *Meis1*, *Muc2*, ***Ppp1r3c***, ***Rad52***, ***Rcan1***, retinoic acid, *Scye1*, *Sp1*, *St8sia1*, *Tgm1*, *TopbpP1*, ***Tubb2c***	Cell cycle, DNA replication, recombination, and repair, cell death
3	*Akt*, *Ap1*, *Bcl2*, Calpain, *Egfr*, *Fgf*, ***Fos***, *Fos-Jun*, ***Hmox1***, *Ige*, *Il1*, *Jnk*, ***Jun***, *Kras*, *Lig3*, *Mapk*, *Mek*, *Mmp*, ***Myc***, ***Net1***, *P38*, *Mapk*, *Pdgf bb*, *Pdgfb*, *Pi3k*, *Pkc(s)*, *Pkg*, *Rar*, *Ras*, *Ras* homolog, *Rock*, *Rxr*, *Sos*, *Stat5a/b*, *Tgf* beta, *Vegf*	Cell death, hepatic system disease, liver necrosis/cell death
4	4-Phenylbutyric acid, *14-3-3*, Calmodulin, *Ccnf*, *Cdkn2a*, *Ck2*, *Cult1*, Cyclin D, *Cyp1a1*, *Ephx1*, *Hira*, Histone h3, *Hnrpa2b1*, *Hsp70*, *Hsp90*, *Hspa1b*, hydrogen peroxide, *Ifng*, *Irf2*, ***Isg20l1***, lipoxin A4, *Lrp1*, ***Mbd1***, *Mcm2*, *Mcm3*, *Meis1*, *Pdk1*, *Pka*, RNA polymerase II, *Ssrp1*, *Supt16h*, *Tp53inp1*, *Ube2e1*, Ubiquitin, *Ung*	Cell cycle, DNA replication, recombination, and repair, cell death
5	*Cdh3*, D *Dpyd*	Cancer, drug metabolism, genetic disorder
(B) DEN 28 d		
1	Adaptor protein 2, Ahr-aryl hydrocarbon-*Arnt*, *Arf*, *Bax*, ***Btg2***, *Casp1*, Caspase, *Cbp/p300*, *Ccng1*, ***Cdkn1a***, *Creb*, Cyclin A, Cyclin E, *E2f*, *Erk1/2*, *Gadd45*, *Gadd45b*, *Gadd45g*, ***Gdf15***, *Gsk3*, *Hist1h1c*, *Hspb1*, *Hspb2*, *Jun/Junb/Jund*, *Mdm2*, *Mek1/2*, *Pak*, *Pdgf*, *Plk2*, *Pml*, *Pmm1*, *Pp2a*, *Rb*, *Stat*, *Trp53*	Cancer, cell cycle, reproductive system disease
2	*Aatf*, *Aldh3a1*, *App*, beta-estradiol, *Ccng2*, *Cyp1a2*, ***Cyp21a1***, *Cyp4a10* (includes EG:1579), *E2f1*, *Fabp5*, ***Gdf15***, *Gyk*, *Glul*, *Hrpt1*, *Hspa1b*, ***Igfbp1***, *Il10*, *Il1b*, *Klf10*, *Klk5*, *Maz*, *Meis1*, *Mt1e*, *Muc2*, *Nr4a3*, *Ppp1r3c*, *Rad52*, *Rcan1*, retinoic acid, *Scye1*, *Sp1*, *St8sia1*, *Tgm1*, *Topbp1*, *Tubb2c*	DNA replication, recombination, and repair, cell death, cell cycle
3	*Akt*, *Ap1*, *Bcl2*, Calpain, *Egfr*, *Fgf*, *Fos*, *Fos-Jun*, *Hmox1*, *Ige*, *Il1*, *Jnk*, *Jun*, *Kras*, *Lig3*, *Mapk*, *Mek*, *Mmp*, *Myc*, *Net1*, *P38 Mapk*, *Pdgf bb*, *Pdgfb*, *Pi3k*, *Pkc(s)*, *Pkg*, *Rar*, *Ras*, *Ras* homolog, *Rock*, *Rxr*, *Sos*, *Stat5a/b*, *Tgf* beta, *Vegf*	Cell death, hepatic system disease, liver necrosis/cell death
4	*14-3-3*, *Bag4*, Calmodulin, *Ccnf*, *Cdkn2a*, *Ck2*, *Cutl1*, *Cyp1a1*, *Dynlrb1*, *Ephx1*, *Hira*, Histone h3, *Hnrpa2b1*, *Hoxb9*, *Hsp70*, *Hsp90*, *Hspa1b*, hydrogen peroxide, *Ifng*, *Isg20l1*, *Lrp1*, *Mbd1*, *Meis1*, *Nol3*, *Pdk1*, *Pka*, *Ppfibp1*, RNA pol2-transcription factor, RNA polymerase II, *Smtn*, *Supt16h*, *Tp53inp1*, *Ube2e1*, Ubiquitin, *Ung*	Cellular development, cellular growth and proliferation, connective tissue development and function
5	*Cdh3*, *Dpyd*	Cancer, drug metabolism, genetic disorder
(C) ENU 4 h		
1	Adaptor protein 2, Ahr-aryl hydrocarbon-*Arnt*, *Arf*, ***Bax***, ***Btg2***, *Casp1*, Caspase, *Cbp/p300*, ***Ccng1***, ***Cdkn1a***, *Creb*, Cyclin A, Cyclin E, *E2f*, *Erk1/2*, *Gadd45*, ***Gadd45b***, *Gadd45g*, ***Gdf15***, *Gsk3*, ***Hist1h1c***, ***Hspb1***, *Hspb2*, *Jun/Junb/Jund*, ***Mdm2***, *Mek1/2*, *Pak*, *Pdgf*, ***Plk2***, *Pml*, *Pmm1*, *Pp2a*, *Rb*, *Stat*, *Trp53*	Cancer, cell cycle, reproductive system disease
2	*Aatf*, *Aldh3a1*, *App*, *Appbp1*, beta-estradiol, *Ccne2*, *Ccng2*, *Cyp1a2*, ***Cyp21a1***, ***Cyp4a10***, *E2f1*, ***Fabp5***, ***Gdf15***, *Gyk*, *Glul*, *Hprt1*, *Hdps1b*, *Igfbp1*, *Il10*, *Il1b*, *Klf10*, *Maz*, *Mis1*, *Muc2*, *Nr4a3*, ***Ppp1r3c***, *Rad52*, ***Rcan1***, retinoic acid, *Scye1*, *Sp1*, *St8sia1*, *Tgm1*, *Topbp1*, ***Tubb2c***	DNA replication, recombination, and repair, cell cycle, cell signaling
3	*Akt*, *Ap1*, *Bcl2*, Calpain, *Egfr*, *Fgf*, ***Fos***, *Fos-Jun*, ***Hmox1***, *Ige*, *IL1*, *Jnk*, ***Jun***, *Kras*, *Lig3*, *Mapk*, *Mek*, *Mmp*, ***Myc***, ***Net1***, *P38*, *Mapk*, *Pdgf bb*, *Pdgfb*, *Pi3k*, *Pkc(s)*, *Pkg*, *Rar*, *Ras*, *Ras* homolog, *Rock*, *Rxr*, *Sos*, *Stat5a/b*, *Tgf* beta, *Vegf*	Cell death, hepatic system disease, liver necrosis/cell death
4	4-phenylbutyric acid, *14-3-3*, Calmodulin, ***Ccnf***, *Cdkn2a*, *Ck2*, *Cult1*, Cyclin D, *Cyp1a1*, *Ephx1*, *Hira*, Histone h3, *Hnrpa2b1*, *Hsp70*, *Hsp90*, *Hspa1b*, hydrogen peroxide, *Ifng*, *Irf2*, ***Isg20l1***, lipoxin A4, *Lrp1*, ***Mbd1***, *Mcm2*, *Mcm3*, *Meis1*, *Pdk1*, *Pka*, RNA polymerase II, *Ssrp1*, *Supt16h*, *Tp53inp1*, *Ube2e1*, Ubiquitin, *Ung*	Cell cycle, DNA replication, recombination, and repair, cell death
5	*Cdh3*, *Dpyd*	Cancer, drug metabolism, genetic disorder
(D) ENU 28 d		
1	Adaptor protein 2, Ahr-aryl hydrocarbon-*Arnt*, *Arf*, *Bax*, *Btg2*, ***Casp1***, Caspase, *Cbp/p300*, *Ccng1*, *Cdkn1a*, *Creb*, Cyclin A, Cyclin E, *E2f*, *Erk1/2*, *Gadd45*, *Gadd45b*, *Gadd45g*, ***Gdf15***, *Gsk3*, *Hist1h1c*, *Hspb1*, ***Hspb2***, *Jun/Junb/Jund*, *Mdm2*, *Mek1/2*, *Pak*, *Pdgf*, *Plk2*, *Pml*, *Pmm1*, *Pp2a*, *Rb*, *Stat*, *Trp53*	Cancer, cell cycle, reproductive system disease
2	*Aatf*, Ahr-aryl hydrocarbon, *App*, *Appbp1*, beta-estradiol, *Ccng2*, *Cd68*, *Cdc45l*, *Cyp1a2*, *Cyp21a1*, *Cyp4a10*, *E2f1*, *Fabp5*, *Folr2*, ***Gdf15***, *Gyk*, *Glul*, *Hprt1*, ***Hspa1b***, *Igfbp1*, *Il10*, *Il1b*, *Klk5*, *Krt16*, *Nr4a3*, *Ppp1r3c*, *Rad52*, *Rcan1*, retinoic acid, *Rrs4x*, *Serpinb9*, *Sp1*, *TacstdA1*, *Tspo*, *Tubb2c*	Cell signaling, molecular transport, small molecule biochemistry
3	*Akt*, *Ap1*, *Bcl2*, Calpain, *Egfr*, *Fgf*, ***Fos***, *Fos-Jun*, *Hmox1*, *Ige*, *IL1*, *Jnk*, *Jun*, *Kras*, *Lig3*, *Mapk*, *Mek*, *Mmp*, *Myc*, *Net1*, *P38*, *Mapk*, *Pdgf bb*, *Pdgfb*, *Pi3k*, *Pkc(s)*, *Pkg*, *Rar*, *Ras*, *Ras* homolog, *Rock*, *Rxr*, *Sos*, *Stat5a/b*, *Tgf* beta, *Vegf*	Cell death, hepatic system disease, liver necrosis/cell death
4	*14-3-3*, *Aco1*, *Asf1b*, *Bag4*, Calmodulin, *Ccnf*, *Cdkn2a*, *Ck2*, *Cyp1a1*, *Dynlrb1*, *Ephx1*, *Hira*, Histone h3, *Hosb9*, *Hsp70*, *Hsp90*, ***Hspa1b***, hydrogen peroxide, *Ifng*, *Isg20l1*, *Lamp1*, *Lrp1*, *Mbd1*, *Nol3*, *Pka*, *Ppfibp1*, RNA pol2-transcription factor, RNA polymerase II, *Rpl21*, *Smtn*, *Sncg*, *Supt16h*, *Ube2e1*, Ubiquitin, ***Ung***	Cellular development, cellular growth and proliferation, connective tissue development and function
5	*Cdh3*, *Dpyd*	Cancer, drug metabolism, genetic disorder

Biologically relevant networks extracted by IPA are shown for gene expression data after (A) DEN-4 h, (B) DEN-28 d, (C) ENU-4 h or (D) ENU-28 d treatment. Bold underlined genes show dose-dependent expression. Thin underlined genes are genes examined in the present study. *Pdgf bb* in Network-3 means *Pdgf* groups of *Pdgfa*, *Pdgfb*, *Pdgfc* and *Pdgfd*. *Hsp70* in Network-4 means *Hsp* groups of *Hspa14 hspa1a*, *Hspa1b*, *Hspa1l*, *Hspa2*, *Hspa4 hspa5*, *Hspa6*, *Hspa7*, *Hspa8*, and *Hspa9*.

was observed, and only *Btg2*, *Cdkn1a* and *Gdf15* showed a dose-dependent increase (Fig. 4A, Network-1). DEN-28 d-Network-2 included several different genes from those in DEN-4 h-Network-2 but had the same primary functions as for DEN-4 h-Network-2, and *Cyp21a1*, *Gdf15* and *Igfbp1* exhibited dose-dependency (Fig. 4A, Network-2). DEN-28 d-Network-3 consisted of the same genes and the same primary functions as for DEN-4 h-Network-3; however, no genes showed dose-dependency (Fig. 4A, Network-3). DEN-28 d-Network-4 contained a few different genes and primary functions from those of DEN-4 h-Network-4, but no genes showed a dose

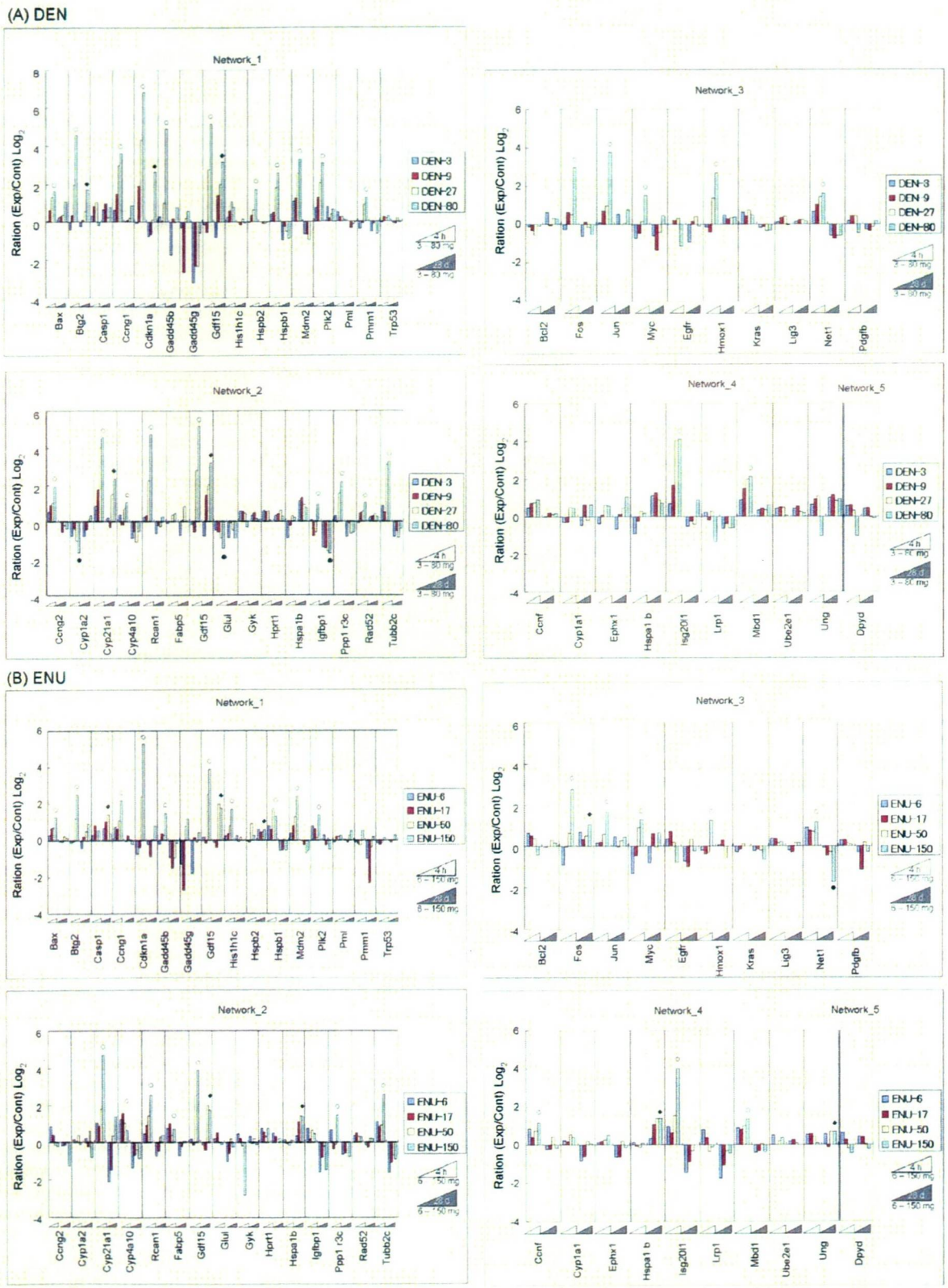

Fig. 4. Dose-dependent gene expression in each network based on different time points. The ratio values (log_2) of genes in each network are shown as bar graphs for DEN treatment (A) or ENU treatment (B). ○ shows a dose-dependent increase at 4 h, ♦ shows a dose-dependent increase at 28 days and ● shows a dose-dependent decrease.

response. DEN-28 d-Network-5 consisted of the same genes and the same top functions as those of DEN-4 h-Network-5, with no genes showing dose-dependency in this study (Fig. 4A, Network-5).

3.2. Dose-dependent alteration of gene expression induced with ENU

3.2.1. Clustering analysis for gene expression

Unsupervised hierarchical clustering results are shown in Fig. 2. The clustering presented three groups (ENU-4 h-Grp-1 to ENU-4 h-Grp-3) and two ungrouped genes for the 4 h time point after administration and four groups (ENU-28 d-Grp-1 to ENU-28 d-Grp-4) for the 28-day time point after administration. As unsupervised hierarchical clustering was performed on 4 h and 28-day data separately, group member genes were different between these two groups.

All four ENU-4 h-Grp-1 genes showed a dose-dependent increase by more than 16–32-fold 4 h after administration. Twenty-four ENU-4 h-Grp-2 genes were suggested to have a gradual dose-dependent increase of less than that of the expression in ENU-4 h-Grp-1.

All three ENU-28 d-Grp-1 genes showed a dose-dependent increase by more than two-fold 28 days after administration. Eight ENU-28 d-Grp-2 genes were suggested to have a gradual dose-dependent increase of less than that of the expression in ENU-28 d-Grp-1. *Net1* in ENU-28 d-Grp-3 showed a dose-dependent decrease of less than 0.3-fold.

Unsupervised *k*-means clustering results are shown in Fig. 3B. In the same way as for DEN, we classified these genes into four clusters based on hierarchical clustering results. For 4 h, four ENU-4 h-Cluster-1 genes exhibited a dose-dependent increase by more than 16-fold. Fourteen ENU-4 h-Cluster-2 genes exhibited a gradual dose-dependent increase as compared to genes in ENU-4 h-Cluster-1. Seven ENU-4 h-Cluster-3 genes showed an increase as a whole, with some atypical features. For 28-day data, seven ENU-28 d-Cluster-1 genes were suggested to have a tendency for a dose-dependent increase. *Net1* in ENU-28 d-Cluster-2 showed a dose-dependent decrease of less than 0.3-fold.

Two kinds of clustering results of ENU treatment are summarized as follows. A total of 29 genes showed a dose-dependent increase or decrease at 4 h or 28 days after administration. For 4 h, a total of 24 genes in ENU-4 h-Grp-1 or ENU-4 h-Grp-2 and ENU-4 h-Cluster-1, ENU-4 h-Cluster-2 or ENU-4 h-Cluster-3 showed a dose-dependent increase ranging from 2-fold to more than 32-fold [*Bax*, *Btg2*, *Ccng1*, *Ccnf*, *Cdkn1a*, *Cyp4a10*, *Cyp21a1*, *Fabp5*, *Fos*, *Gadd45b*, *Gdf15*, *Hist1h1c*, *Hmox1*, *Hspb1*, *Isg20l1*, *Jun*, *Mbd1*, *Mdm2*, *Myc*, *Net1*, *Plk2*, *Ppp1r3c*, *Rcan1* and *Tubb2c*].

For 28 days, a total of eight genes were classified as dose–response genes. Four genes in ENU-28 d-Grp-1, ENU-28 d-Grp-2, and ENU-28 d-Cluster-1 showed a dose-dependent increase of more than 2-fold [*Casp1*, *Fos*, *Gdf15* and *Hspa1b*]. Another three genes in ENU-28 d-Grp2 and ENU-28 d-Cluster-1 showed less than a two-fold increase [*Gstk1*, *Hspb2* and *Ung*]. *Net1* in ENU-28 d-Grp-3 and ENU-28 d-Cluster-2 showed a dose-dependent decrease of less than 0.3-fold.

3.2.2. Identification of biologically relevant networks for ENU treatment

ENU numerical data for all 51 examined genes were also analyzed by IPA for 4 h and 28-day data, and five gene networks were extracted (3). In total, the gene expression pattern for ENU was similar to the pattern for DEN; however, some differences were observed.

For 4 h, ENU-4 h-Network-1 consisted of the same genes and the same top functions as for DEN-4 h-Network-1, and 10 of these genes showed a dose-dependent increase [*Bax*, *Btg2*, *Ccng1*, *Cdkn1a*, *Gadd45b*, *Gdf15*, *Hist1h1c*, *Hspb1*, *Mdm2* and *Plk2*] (Fig. 4B, Network-1). Network-1 was the most active network for ENU-4 h. ENU-4 h-Network-2 (DNA replication, recombination, repair, cell cycle and cell signaling) included a different primary function from that of DEN-4 h-Network-2 and a few different genes from those for DEN, and seven genes showed a dose-dependent increase [*Cyp21a1*, *Cyp4a10*, *Fabp5*, *Gdf15*, *Ppp1r3c*, *Rcan1* and *Tubb2c*] (Fig. 4B, Network-2). ENU-4 h-Network-3 consisted of the same genes and the same top functions as those for DEN-4 h-Network-3, and five genes showed a dose-dependent increase [*Fos*, *Hmox1*, *Jun*, *Myc* and *Net1*] (Fig. 4B, Network-3). ENU-4 h-Network-4 also consisted of the same genes and the same top functions as those for DEN, and three genes showed a dose-dependent increase [*Ccnf*, *Isg20l1* and *Mbd1*] (Fig. 4B, Network-4). ENU-4 h-Network-5 consisted of the same genes and the same top functions as those for DEN-4 h-Network-5, but no genes showed a dose–response in this study (Fig. 4B, Network-5).

Network-1, Network-3 and Network-5 consisted of common genes and common top functions for both 4 h and 28 days and for both DEN and ENU. For 28 days, three genes in ENU-28 d-Network-1 showed a dose-dependent increase [*Casp1*, *Gdf15* and *Hspb2*] (Fig. 4B, Network-1). ENU-28 d-Network-2 included 10 different genes from those for ENU-4 h-Network-2 and had different top functions (cell signaling, molecular transport and small molecule biochemistry) from those of DEN-4 h-Network-2, DEN-28 d-Network-2 and ENU-4 h-Network-2, and 2 genes showed a dose-dependent increase [*Gdf15 and Hspa1b*] (Fig. 4B, Network-2). *Fos* and *Net1* in ENU-28 d-Network-3 showed a dose–response (Fig. 4B, Network-3). ENU-28 d-Network-4 (Table 2D) included different primary functions (cellular development, cellular growth, proliferation and connective tissue development and function) and 10 different genes from ENU-4 h-Network-4; two genes showed a dose–response [*Hspab1* and *Ung*]. ENU-28 d-Network-5 consisted of the same genes and the same top functions as those of DEN-4 h-Network-5, while no genes showed a dose–response in this study (Fig. 4A, Network-5).

4. Discussion

We examined the dose-dependency of gene expression changes for 51 genes in mouse liver treated with two *N*-nitroso genotoxic hepatocarcinogens, DEN and ENU, by qPCR at early times after administration. We selected 51 candidate genes based on our previous results of Affymetrix GeneChip Mu74AV2 and original DNA microarray of samples after treatment with DEN, dimethylnitrosamine, dipropylnitrosamine, ENU, *o*-aminoazotoluene, 7,12-dimethylbenz[*a*]anthracene, dibenzo[*a*,*l*]pyrene, phenobarbital and ethanol in our JEMS/MMS/Toxicogenomics group collaborative study. Because only a single dose was used for each chemical in the previous study, we examined dose-dependency in gene expression changes in this study using two representative chemicals. We showed distinct dose-dependency of gene expression changes induced by DEN and ENU; these changes associated with cancer, cell cycle arrest, DNA replication, recombination, repair and cell death not only at 4 h, but also, for some, at 28 days after administration. Similar gene expression changes between DEN and ENU were characteristic. Twenty-one genes exhibited a distinct dose-dependent increase at 4 h for both carcinogens [*Bax*, *Btg2*, *Ccng1*, *Cdkn1a*, *Cyp4a10*, *Cyp21a1*, *Fos*, *Gadd45b*, *Gdf15*, *Hmox1*, *Hspb1*, *Isg20l1*, *Jun*, *Mbd1*, *Mdm2*, *Myc*, *Net1*, *Plk2*, *Ppp1r3c*, *Rcan1* and *Tubb2c*], although the gene expression changed after ENU was generally weaker relative to that after DEN. The results were consistent with a previous report that showed more DNA lesions with DEN than with ENU a few hours after administration [6]. Only *Gdf15* showed a dose-dependent increase at 28 days for

both carcinogens. An additional seven different genes for DEN and eight genes for ENU also showed dose-dependency. *Ccng2*, *Hspb2*, *Igfbp1*, *Pmm1* and *Rad52* showed a dose-dependent increase and *Cyp1a2* and *Glul* showed a dose-dependent decrease 4 h after administration only with DEN. *Btg2*, *Cdkn1a* and *Cyp21a1* showed a dose-dependent increase 28 days after administration only with DEN and these genes also showed a dose–response at 4 h. *Ccnf*, *Fabp5* and *Hist1h1c* showed a dose-dependent increase 4 h after administration only with ENU. *Casp1*, *Fos*, *Gstk1*, *Hspa1b*, *Hspb2* and *Ung* showed a dose-dependent increase 28 days after administration only with ENU. *Ccnf* in DEN-4 h and *Bax* and *Ephx1* in DEN-28 d showed equivocal changes. We only observed several dose-dependent decreases in expression of genes [*Cyp1a2*, *Glul*, *Igfbp1* and *Net1*] after DEN and ENU in the present experimental conditions.

In the previous study [10], gene expression changes in number and degree were observed to peak at 4 h after administration and were lower at 20 h, 14 and 28 days. In the present study, we investigated the gene expression pattern at two different time points: 4 h, during production of many DNA lesions, and 28 days, during fixing of mutations [6]. We expected to observe the earliest and most varied effects in many cells in the liver, including DNA lesions, 4 h after administration. It was presumed that most of the DNA-damaged cells would be repaired, that some of the damaged cells would die and that only a few cells would progress to carcinogenesis. We reasoned that it would be useful to examine the earliest various effects to understand the potential gene-altering ability of carcinogens. The second time point, 28 days, is the time by which most mutations are fixed, the remainder of which would be related to carcinogenesis. We expected to observe gene expression changes which would reflect the effects of mutation at 28 days. The role of genes with altered expression might be different even if expression of the same gene was changed at 4 h and 28 days.

In addition, we examined gene networks using IPA to clarify interactions between genes with altered expression. IPA identified five networks of genes regulated at 4 h after DEN and ENU treatment (Table 3 and Fig. 4). As for DEN, 11 dose-dependent genes [*Bax*, *Btg2*, *Ccng1*, *Cdkn1a*, *Gadd45b*, *Gdf15*, *Hspb1*, *Hspb2*, *Mdm2*, *Plk2* and *Pmm1*] belonged to Network-1 (cancer and cell cycle) and the other 11 dose-dependent genes [*Ccng2*, *Cyp1a2*, *Cyp4a10*, *Cyp21a1*, *Gdf15*, *Glul*, *Igfbp1*, *Ppp1r3c Rad52*, *Rcan1* and *Tubb2c*] belonged to Network-2 (cell cycle, cell death, DNA replication, recombination and repair). In detail, *Gdf15* was extracted in both Network-1 and Network-2. As for ENU, 10 dose-dependent genes [*Bax*, *Btg2*, *Ccng1*, *Cdkn1a*, *Gadd45b*, *Gdf15*, *Hist1h1c*, *Hspb1*, *Mdm2* and *Plk2*] belonged to the same Network-1 and 7 dose-dependent genes [*Cyp21a1*, *Cyp4a10*, *Fabp5*, *Gdf15*, *Ppp1r3c*, *Rcan1* and *Tubb2c*] belonged to a different Network-2 (DNA replication, recombination and repair, and cell cycle and cell signaling). *Hspb2* and *Pmm1* showed dose–responses only in DEN-4 h-Network-1 and *Hist1h1c* showed a dose–response only in ENU-4 h-Network-1. [Cell death] in DEN-4 h-Network-2 was replaced with [Cell signaling] in ENU-4 h-Network-2. *Ccng2*, *Cyp1a2*, *Glul*, *Igfbp1* and *Rad52* showed dose–responses only in DEN-4 h-Network-2 and *Fabp5* showed a dose–response only in ENU-4 h-Network-2. This difference in Network-2 was the most remarkable difference between the effects of DEN and ENU in the present study. The top functions of Network-1 and Network-2 were characteristic networks for DEN-4 h and ENU-4 h, being typical of carcinogenic compounds. As for 28 days, IPA also identified five networks of genes, however, only a few genes showed a dose–response with DEN and ENU. As for DEN, three dose-dependent genes [*Btg2*, *Cdkn1a* and *Gdf15*] belonged to Network-1 and two genes [*Cyp21a1* and *Gdf15*] belonged to Network-2. As for ENU, three dose-dependent genes [*Casp1*, *Gdf15* and *Hspb2*] belonged to Network-1, [*Gdf15* and *Hspa1b*] belonged to Network-2, [*Fos* and *Net1*] belonged to Network-3 and [*Hspa1b* and *Ung*] belonged to Network-4. The present results suggested similar functions for *N*-nitroso carcinogens DEN and ENU, with several differences. We have examined effects of other genotoxic and non-genotoxic carcinogens in mouse liver at 4 h and have generated various networks for various carcinogens (unpublished).

We showed that Network-1 was associated with cancer and the cell cycle. To understand more detailed functions, we examined a major canonical pathway for each network. A major canonical pathway in Network-1 was *p53* signaling. The increase of *Cdkn1a*, *Ccng1* and *Gadd45* demonstrated cell cycle arrest. The expression pattern (Fig. 4) at 4 h showed that cell cycle arrest would proceed, to then be released by day 28. Both *p53* and *Bax* were associated with initiation of apoptosis.

In the same way, a major canonical pathway in Network-2 was aryl hydrocarbon receptor signaling [14]. Furthermore, aryl hydrocarbon receptor signaling as an adaptive response was manifested as the induction of xenobiotic metabolizing enzymes; *Cyp1a2*, *Cyp21a1* and *Cyp4a10* take part in this pathway. *Cyp21a1* also takes part in biosyntheses of steroid hormones [15]. Inflammation of the liver is controlled at 28 days after administration because steroid hormones function to suppress inflammation.

Growth/differentiation factor-15 (*Gdf15*) was the only gene whose expression increased at 4 h and 28 days of both DEN and ENU and belonged to Network-1 and Network-2 at 4 h and 28 days of DEN and ENU. *Gdf15* is a divergent Tgf-beta family member that is expressed following liver injury and carcinogen exposure [16]. *Gdf15* in liver is rapidly and dramatically up-regulated following various surgical and chemical treatments that cause acute liver injury and regeneration [17].

A major canonical pathway in Network-3 was platelet-derived growth factor (*Pdgf*) signaling. *Pdgfb*, *Kras*, *Jun*, *Fos* and *Myc* may be associated with *Pdgf* signaling. In this canonical pathway, *Pdgfb* phosphorylates other proteins and activates the downstream genes *Kras*, *Jun*, *Fos* and *Myc* [18–21], one reason why *Pdgfb* expression did not change significantly (Fig. 3A, Cluster-4).

Our results show that most differentially expressed genes at 4 h and 28 days exhibited a dose–response. Only a few genes, *Dpyd*, *Egfr*, *Lrp1* and *Ung* for DEN at 4 h; *Gyk* for ENU at 4 h; and *Ccng2* for ENU at 28 days showed atypical gene expression changes at the highest dose. These changes may be toxicity-related. *Dpyd* is associated with pyrimidine metabolism. *Egfr* is associated with cell proliferation. *Lrp* plays a clear protective role in atherogenesis. *Ung* is associated with DNA repair. Their decrease may show the loss of cell maintenance because hepatocytes will have received much lethal damage at the highest dose. *Gyk* is associated with xenobiotic metabolism signaling. It has been reported that glycerol kinase deficiency is involved in lipid metabolism, carbohydrate metabolism, and insulin signaling [22]. Indeed, it has been reported that type 2 diabetes is caused by ENU but not by DEN [23]. Unlike classical cyclins that promote cell cycle progression, cyclin G2 blocks cell cycle entry. The decrease of *Ccng2* mRNA may promote cell cycle progression.

Previously, we reported differential gene expression induced by two *N*-nitroso genotoxic hepatocarcinogens, DEN and dipropylnitrosamine (DPN) as compared to phenobarbital and ethanol in mouse liver examined with an original oligonucleotide microarray and qPCR [10]. We observed 11 differentially expressed genes 4 h after administration, including 7 tumor suppressor *Trp53* target genes, *Bax*, *Ccng1*, *Cdkn1a*, *Hspb2/Hsp27*, *Jun*, *Mdm2*, and *Plk2/Snk*; the other genes were *Ccnf*, *Hmox1*, *Mbd1*, and *Rad52*. Furthermore, some degree of differential gene expression of *Ccng1*, *Cdkn1a* and *Plk2/Snk* was observed 28 days after administration. In the present study, we selected 51 candidate genes (Table 1) based on our original DNA microarray and Affymetrix GeneChip Mu74AV2 data (not published) on seven genotoxic carcinogens, phenobarbital and ethanol. The present results show that 28 genes for

DEN and 29 genes for ENU exhibited dose-dependent differential expression. Differential gene expression was observed commonly at least for *Bax*, *Ccng1*, *Cdkn1a*, *Hmox1*, *Jun*, *Mbd1*, *Mdm2* and *Plk2* with these three *N*-nitroso carcinogens (DEN, DPN and ENU). As we expanded qPCR analysis from 14 genes in the previous study [10] to 51 genes in the present study, we could show complex gene networks by IPA. Twenty genes, *Btg2*, *Casp1*, *Ccng2*, *Cyp4a10*, *Cyp21a1*, *Ephx1*, *Gadd45b*, *Gdf15*, *Glul*, *Gstk1*, *Hspa1b*, *Hspb1*, *Igfbp1*, *Isg20l1*, *Net1*, *Pmm1*, *Ppp1r3c*, *Rcan1*, *Tubb2c* and *Ung*, which showed dose–responses in the present study, were newly examined.

We examined only pooled materials from five mice in the present study. However, we already reported that at least five genes (*Gapdh*, *Jun*, *Ccng1*, *Hspb2/Hsp27* and *Rad52*) exhibited only small inter-individual mouse gene expression variation [10] with DEN treatment after 4 h and 28 days. Additional study showed that *Bax*, *Hmox1*, *Mbd1*, *Mdm2* and *Plk2* also exhibited only small inter-individual gene expression variation with DEN treatment at 4 h and 28 days (unpublished data).

We will continue further studies on other types of chemicals for characterizing mutagenic and carcinogenic compounds; these data will be useful for chemical risk assessment and for furthering our understanding of the underlying biological processes.

Conflict of interest

We have not any conflicting interest include employment, consultancies, stock ownership, honoraria, paid expert testimony, patent applications/registrations, and grants or other funding.

Acknowledgements

This work was partly supported by KAKENHI (18310047) (C. Furihata, T. Watanabe and T. Suzuki), The Ministry of Education, Culture, Sports, Science and Technology, Japan and a High-Tech Research Center project for private universities with a matching fund subsidy from The Ministry of Education, Culture, Sports, Science and Technology, Japan (C. Furihata).

References

[1] B.A. Diwan, H. Meier, Carcinogenic effects of a single dose of diethylnitrosamine in three unrelated strains of mice: genetic dependence of the induced tumor types and incidence, Cancer Lett. 1 (1976) 249–253.
[2] A.P. Kyriazis, S.D. Vesselinovitch, Transplantability and biological behavior of mouse liver tumors induced by ethylnitrosourea, Cancer Res. 33 (1973) 332–338.
[3] J.A. Swenberg, M.C. Dyroff, M.A. Bedell, J.A. Popp, N. Huh, U. Kirstein, M.F. Rajewsky, O4-ethyldeoxythymidine, but not O6-ethyldeoxyguanosine, accumulates in hepatocyte DNA of rats exposed continuously to diethylnitrosamine, Proc. Natl. Acad. Sci. U.S.A. 81 (1984) 1692–1695.
[4] J.L. Yang, P.C. Lee, S.R. Lin, J.G. Lin, Comparison of mutation spectra induced by N-ethyl-N-nitrosourea in the hprt gene of Mer+ and Mer– diploid human fibroblasts, Carcinogenesis 15 (1994) 939–945.
[5] T. Suzuki, M. Hayashi, T. Sofuni, Initial experiences and future directions for transgenic mouse mutation assays, Mutat. Res. 307 (1994) 489–494.
[6] E.J. Mientjes, A. Luiten-Schuite, E. van der Wolf, Y. Borsboom, A. Bergmans, F. Berends, P.H. Lohman, R.A. Baan, J.H. van Delft, DNA adducts, mutant frequencies, and mutation spectra in various organs of lambda lacZ mice exposed to ethylating agents, Environ. Mol. Mutagen. 31 (1998) 18–31.
[7] J.F. Waring, R.A. Jolly, R. Ciurlionis, P.Y. Lum, J.T. Praestgaard, D.C. Morfitt, B. Buratto, C. Roberts, E. Schadt, R.G. Ulrich, Clustering of hepatotoxins based on mechanism of toxicity using gene expression profiles, Toxicol. Appl. Pharmacol. 175 (2001) 28–42.
[8] M.J. Bartosiewicz, D. Jenkins, S. Penn, J. Emery, A. Buckpitt, Unique gene expression patterns in liver and kidney associated with exposure to chemical toxicants, J. Pharmacol. Exp. Ther. 297 (2001) 895–905.
[9] M. Provenzano, S. Mocellin, Complementary techniques: validation of gene expression data by quantitative real time PCR, Adv. Exp. Med. Biol. 593 (2007) 66–73.
[10] T. Watanabe, K. Tobe, Y. Nakachi, Y. Kondoh, M. Nakajima, S. Hamada, C. Namiki, T. Suzuki, S. Maeda, A. Tadakuma, M. Sakurai, Y. Arai, A. Hyogo, M. Hoshino, T. Tashiro, H. Ito, H. Inazumi, Y. Sakaki, H. Tashiro, C. Furihata, Differential gene expression induced by two genotoxic *N*-nitroso carcinogens, phenobarbital and ethanol in mouse liver examined with oligonucleotide microarray and quantitative real-time PCR, Gene Environ. 29 (2007) 115–127.
[11] K. Sekihashi, A. Yamamoto, Y. Matsumura, S. Ueno, M. Watanabe-Akanuma, F. Kassie, S. Knasmüller, S. Tsuda, Y.F. Sasaki, Comparative investigation of multiple organs of mice and rats in the comet assay, Mutat. Res. 517 (2002) 53–75.
[12] S. Madle, S.W. Dean, U. Andrae, G. Brambilla, B. Burlinson, D.J. Doolittle, C. Furihata, T. Hertner, C.A. McQueen, H. Mori, Recommendations for the performance of UDS tests in vitro and in vivo, Mutat. Res. 312 (1994) 263–285.
[13] A. Sturn, J. Quackenbush, Z. Trajanoski, Genesis: Cluster analysis of microarray data, Bioinformatics 18 (2002) 207–208.
[14] D.W. Kim, L. Gazourian, S.A. Quadri, R. Romieu-Mourez, D.H. Sherr, G.E. Sonenshein, The RelA NF-kappaB subunit and the aryl hydrocarbon receptor (AhR) cooperate to transactivate the Myc promoter in mammary cells, Oncogene 19 (2000) 5498–5506.
[15] J. Gonçalves, A. Friães, L. Moura, Congenital adrenal hyperplasia: focus on the molecular basis of 21-hydroxylase deficiency, Expert Rev. Mol. Med. 9 (2007) 1–23.
[16] T.A. Zimmers, X. Jin, J.C. Gutierrez, C. Acosta, I.H. McKillop, R.H. Pierce, L.G. Koniaris, Effect of in vivo loss of GDF-15 on hepatocellular carcinogenesis, J. Cancer Res. Clin. Oncol. 134 (2008) 753–759.
[17] E.C. Hsiao, L.G. Koniaris, T. Zimmers-Koniaris, S.M. Sebald, T.V. Huynh, S.J. Lee, Characterization of growth-differentiation factor 15, a transforming growth factor beta superfamily member induced following liver injury, Mol. Cell. Biol. 20 (2000) 3742–3751.
[18] S. Svegliati, R. Cancello, P. Sambo, M. Luchetti, P. Paroncini, G. Orlandini, G. Discepoli, R. Paterno, M. Santillo, C. Cuozzo, S. Cassano, E.V. Avvedimento, A. Gabrielli, Platelet-derived growth factor and reactive oxygen species (ROS) regulate Ras protein levels in primary human fibroblasts via ERK1/2. Amplification of ROS and Ras in systemic sclerosis fibroblasts, J. Biol. Chem. 280 (2005) 36474–36482.
[19] J.W. Tullai, M.E. Schaffer, S. Mullenbrock, S. Kasif, G.M. Cooper, Identification of transcription factor binding sites upstream of human genes regulated by the phosphatidylinositol 3-kinase and MEK/ERK signaling pathways, J. Biol. Chem. 279 (2004) 20167–20177.
[20] A.J. Kudla, M.L. John, D.F. Bowen-Pope, B. Rainish, B.B. Olwin, A requirement for fibroblast growth factor in regulation of skeletal muscle growth and differentiation cannot be replaced by activation of platelet-derived growth factor signaling pathways, Mol. Cell. Biol. 15 (1995) 3238–3246.
[21] P.A. Bromann, H. Korkaya, C.P. Webb, J. Miller, T.L. Calvin, S.A. Courtneidge, Platelet-derived growth factor stimulates Src-dependent mRNA stabilization of specific early genes in fibroblasts, J. Biol. Chem. 280 (2005) 10253–10263.
[22] L. Rahib, N.K. MacLennan, S. Horvath, J.C. Liao, K.M. Dipple, Glycerol kinase deficiency alters expression of genes involved in lipid metabolism, carbohydrate metabolism, and insulin signaling, Eur. J. Hum. Genet. 15 (2007) 646–657.
[23] A.A. Toye, L. Moir, A. Hugill, L. Bentley, J. Quarterman, V. Mijat, T. Hough, M. Goldsworthy, A. Haynes, A.J. Hunter, M. Browne, N. Spurr, R.D. Cox, A new mouse model of type 2 diabetes, produced by N-ethyl-nitrosourea mutagenesis, is the result of a missense mutation in the glucokinase gene, Diabetes 53 (2004) 1577–1583.

Am J Physiol Cell Physiol 298: C140–C148, 2010.
First published July 15, 2009; doi:10.1152/ajpcell.00050.2009.

Continuous mild heat stress induces differentiation of mammalian myoblasts, shifting fiber type from fast to slow

Tetsuo Yamaguchi,[1] Takayoshi Suzuki,[2] Hideaki Arai,[1] Shihori Tanabe,[3] and Yoriko Atomi[4]

[1]Department of Life Sciences, Graduate School of Arts and Sciences, University of Tokyo, Meguro-ku, Tokyo; [2]Division of Genetics and Mutagenesis and [3]Division of Cellular and Gene Therapy Products, National Institute of Health Sciences, Setagaya-ku, Tokyo; and [4]Department of Technology, University of Tokyo, Bunkyo-ku, Tokyo, Japan

Submitted 27 January 2009; accepted in final form 13 July 2009

Yamaguchi T, Suzuki T, Arai H, Tanabe S, Atomi Y. Continuous mild heat stress induces differentiation of mammalian myoblasts, shifting fiber type from fast to slow. *Am J Physiol Cell Physiol* 298: C140–C148, 2010. First published July 15, 2009; doi:10.1152/ajpcell.00050.2009.— Local hyperthermia has been widely used as physical therapy for a number of diseases such as inflammatory osteoarticular disorders, tendinitis, and muscle injury. Local hyperthermia is clinically applied to improve blood and lymphatic flow to decrease swelling of tissues (e.g., skeletal muscle). As for muscle repair following injury, the mechanisms underlying the beneficial effects of hyperthermia-induced muscle repair are unknown. In this study, we investigated the direct effects of continuous heat stress on the differentiation of cultured mammalian myoblasts. Compared with control cultures grown at 37°C, incubation at 39°C (continuous mild heat stress; CMHS) enhanced myotube diameter, whereas myotubes were poorly formed at 41°C by primary human skeletal muscle culture cells, human skeletal muscle myoblasts (HSMMs), and C2C12 mouse myoblasts. In HSMMs and C2C12 cells exposed to CMHS, mRNA and protein levels of myosin heavy chain (MyHC) type I were increased compared with the control cultures. The mRNA level of MyHC IIx was unaltered in HSMMs and decreased in C2C12 cells, compared with cells that were not exposed to heat stress. These results indicated a fast-to-slow fiber-type shift in myoblasts. We also examined upstream signals that might be responsible for the fast-to-slow shift of fiber types. CMHS enhanced the mRNA and protein levels of peroxisome proliferator-activated receptor-γ coactivator (PGC)-1α in HSMMS and C2C12 cells but not the activities of MAPKs (ERK1/2 and p38 MAPK) in HSMMs and C2C12 cells. These data suggest that CMHS induces a fast-to-slow fiber-type shift of mammalian myoblasts through PGC-1α.

fiber-type shift; PGC-1α; myosin heavy chain; hormesis

TEMPERATURE STRONGLY INFLUENCES growth processes. The effects of heat stress on cellular activities depend on the strength and duration of the applied stress. Hyperthermia has been widely used as a physical therapy for a number of diseases such as inflammatory osteoarticular disorders, tendinitis, and muscle injury, as well as malignant tumor (19, 30, 43, 49). Muscle injuries represent a major part of sports injuries. Local hyperthermia is reported to be a safe and reliable modality for the treatment of muscle injuries in humans (19, 43). Furthermore, local hyperthermia facilitates the healing process by producing blood vessel dilation, thereby enhancing local blood flow and decreasing edema (19). In contrast, little is known about the mechanisms underlying hyperthermia-induced repair of muscle cells following injury.

Several lines of evidence indicate that fever-range elevation of temperature or mild heat stress may be beneficial to living cells by positively regulating cell proliferation and differentiation (11, 33, 42). Fever seems to provoke an effective immune response through the facilitation of T cell proliferation and activation (11, 33). Furthermore, incubation at 39°C induces proliferation and differentiation of osteoprogenitor cells (42). However, the effects of febrile-range heat stress on myotube formation have not yet been determined.

Skeletal muscle develops from the initial fusion of singly nucleated myoblasts to each other to form myotubes. Myogenesis is regulated by the sequential expression of myogenic regulatory factors (MRFs), a group of basic helix-loop-helix transcription factors that includes MyoD, Myf5, myogenin, and MRF4 (44). MyoD and Myf5 are the primary MRFs required for the formation, proliferation, and survival of myoblasts, whereas myogenin and MRF4 act late during myogenesis and activate the expression of important muscle-specific genes, such as myosin heavy chain (MyHC) and creatine kinase (1, 25). Hugh et al. (15) reported that MyoD is prevalent in fast-twitch muscles and myogenin in slow-twitch muscles.

Muscle fibers are dynamic structures capable of altering their phenotype. Under certain conditions, changes can be induced in MyHC isoform expression, shifting either fast to slow or slow to fast. Increased neuromuscular activity, mechanical loading, and hypothyroidism are conditions that induce a fast-to-slow shift, whereas reduced neuromuscular activity, mechanical unloading, and hyperthyroidism cause a shift to the slow-to-fast direction (35). Several signaling pathways regulate the skeletal muscle fiber-type shift. A fast-to-slow fiber-type shift includes pathways that involve the peroxisome proliferator-activated receptor-α coactivator (PGC)-1α (21), Ras/ERK-1/2 (31), calcineurin (32), and CaMK IV (48). In contrast, p38 MAPK controls the activity of the MyHC IIx promoter in C2C12 mouse myoblasts and primary rabbit skeletal myotubes (27).

In the present investigation, we examined the direct effect of continuous heat stress on the differentiation of human skeletal muscle myoblasts (HSMMs) and C2C12 cells under cell culture conditions. We found that incubation at 39°C increased myotube diameter, whereas incubation at 41°C resulted in poorly formed myotubes in both HSMMs and C2C12 cells. To identify whether heat stress affected the fiber-type shift of mammalian myoblasts, we investigated changes in the protein and gene expression levels of MyHC isoforms and PGC-1α, as well as changes in the activities of MAPKs (ERK1/2 and p38

Addresses for reprint requests and other correspondence: T. Yamaguchi, Dept. of Life Sciences, The Graduate School of Arts and Sciences, The Univ. of Tokyo, 3-8-1, Komaba, Meguro-ku, Tokyo 153-8902, Japan (e-mail: tetsuo-yama@abeam.ocn.ne.jp); Y. Atomi, Radioisotope Center, The University of Tokyo, 2-11-16, Yayoi, Bunkyo-ku, Tokyo, 113-0032, Japan (e-mail: atomi@bio.c.u-tokyo.ac.jp).

MAPK). We report that a mild increase in temperature induced expression of PGC-1α and oxidative MyHC isoforms.

MATERIALS AND METHODS

Materials

C2C12 cells were a generous gift from T. Endo (Chiba University, Chiba, Japan). For primary culture of human skeletal muscle cells, muscle samples were obtained surgically from the middle portion of the vastus lateralis muscle of a 72-yr-old female patient undergoing orthopedic surgery during spinal anesthesia. The patient had no previous record of muscular disease, arthritis, autoimmune disease, heart disease, cancer, or metabolic disorders. The muscle samples were obtained at the onset of the surgical procedures (hemi-hip arthroplasty for femoral neck fracture). The sampling site was not within the primary surgical area. The study was approved by the ethical committee of the University of Tokyo and conformed to the standards set by the Declaration of Helsinki. After the subject had been fully informed of the goal of the experiments and of the risks involved in the procedure, written informed consent was obtained before admission in the study. We also used commercially available HSMMs of normal human quadriceps muscle obtained from three males, 13, 16, and 22 yr of age (CC-2580; Lonza Walkersville, Walkersville, MD).

DMEM was purchased from Nissui (Tokyo, Japan). FBS was purchased from Sigma-Aldrich (St. Louis, MO). L-Glutamine, trypsin-EDTA, fungizone, horse serum (HS), and penicillin-streptomycin-neomycin (PSN) antibiotic mixture were purchased from GIBCO (Grand Island, NY). Ultroser G (UG) was purchased from Biosepra (Cergy, France). Collagen type I-coated 60-mm dishes and cover glasses (25-mm type) were purchased from Iwaki (Tokyo, Japan). All other chemicals and reagents were purchased from Wako Pure Chemical Industries (Osaka, Japan). DMEM was supplemented with 2 mM L-glutamine, 10 mM HEPES buffer, and 0.25 μg/ml fungizone.

Antibody against heat shock protein (HSP) 70 was purchased from Stressgen Biotechnologies (San Diego, CA). Antibodies against MyoD (M-318), myogenin (F5D), PGC-1α, p38 MAPK, and phospho-ERK1/2 recognizing p-Tyr-204 were purchased from Santa Cruz Biotechnology (Santa Cruz, CA). Antibodies against MyHC (type I, clone NOQ7.5.4D; type II, clone MY-32), and β-actin (clone AC-15) were purchased from Sigma-Aldrich. Antibody against MyHC type IIa (clone A4.74) was purchased from American Type Culture Collection (Manassas, VA). Antibodies against ERK1/2 and phospho-p38 MAPK recognizing p-Thr-180/Tyr-192 were purchased from Cell Signaling Technology (Beverly, MA). Rhodamine-conjugated Goat-anti-mouse IgG was purchased from Chemicon International (Temecula, CA).

Primary Culture Of Human Skeletal Muscle Cells

Subjects and muscle samples. Primary culture of human skeletal muscle cells was established as described by Gaster (10). In brief, muscle tissue was minced, washed, and enzymatically dissociated for 45 min with 0.05% trypsin-EDTA. After 10% FBS was added to inhibit trypsin, the dissociated cells were centrifuged at 1,000 rpm for 5 min. Myoblasts were isolated from contaminating fibroblasts as follows: the suspended mixed cells were plated on a non-collagen-coated dish for 20 min, to which fibroblasts rapidly attach, leaving myoblasts suspended in the medium. The attached fibroblasts were discarded, and suspended myoblasts were plated in a new dish. The initial growth medium was DMEM supplemented with 10% FBS incubated at 37°C, 5% CO_2-95% air. After 24 h, cell debris and nonadherent cells were removed using DMEM growth medium supplemented with 2% FBS, 2% UG, and 0.1% PSN antibiotic mixture. When a 70–80% growth confluency was reached, the cells were switched to differentiation medium containing 1% FBS, 1% UG, and 0.1% PSN antibiotic mixture in DMEM.

Culture of HSMMs. HSMMs from three donors were cultured separately on collagen type I-coated dishes using skeletal muscle basal medium-2 (SkBM-2) supplemented with the SkBM-2 SingleQuots kit according to the manufacturer's protocol (Lonza Walkersville). When the cells reached 70–80% confluency, the medium was changed to DMEM containing 2% HS.

Culture of C2C12 cells. C2C12 cells were cultured on collagen type I-coated dishes using DMEM supplemented with 10% heat-inactivated FBS. When the cells reached 70–80% confluency, the medium was changed to differentiation medium containing 2% HS in DMEM.

Heat Stress Exposure

Cells were seeded in the growth medium and incubated at 37°C until they reached 70–80% confluency. The medium was then changed to the differentiation medium to induce myotube formation. At the same time, the culture temperature was set at 37, 39, and 41°C for 1–72 h (see Fig. 1). The cell culture was incubated in water-jacketed incubators with humidified air mixed with 5% CO_2. The culture temperature was measured with a thermometer, confirming ±0.1°C precision.

Western Blot Analysis

We investigated the expression level of each protein in HSMMs or in C2C12 cells after heat stress. Cells were washed twice with PBS and lysed with 2× Laemmli sample buffer. The protein concentrations were quantified using the DC protein assay (Bio-Rad Laboratories, Hercules, CA) with BSA as standards.

Aliquots containing 10 μg of total protein were separated using 8–12% SDS polyacrylamide electrophoresis and electrophoretically transferred to a nitrocellulose membrane (Amersham International, Am-

Table 1. *Real-time RT-PCR primers*

Genes	Forward Primer	Reverse Primer
Human		
MyHC I	5′-ACAAGCTCCAGCTAAAGCTC-3′	5′-TCAAGATGTCCCAAAGCTAC-3′
MyHC IIa	5′-AAGGATACCCAGATCCACC-3′	5′-CTCAGCATTACGCTTTTGC-3′
MyHC IIx	5′-AAGAGCAGGGAGGTTCACAC-3′	5′-TTATCTCCAAAAGTCATAAGTACA-3′
PGC-1α	5′-GCTTTCTGGGTGGACTCAAGT-3′	5′-TCTAGTGTCTCTGTGAGGACTG-3′
β-Actin	5′-ACTCTTCCAGCCTTCCTTC-3′	5′-ATCTCCTTCTGCATCCTGTC-3′
Mouse		
MyHC I	5′-CCTTGGCACCAATGTCCCGGCTC-3′	5′-GAAGCGCAATGCAGAGTCGGTC-3′
MyHC IIa	5′-ATGAGCTCCGACGCCGAG-3′	5′-TCTGTTAGCATGAACTGCTAGCCG-3′
MyHC IIx	5′-AAGGAGCAGGACACCAGCGCCCA-3′	5′-ATCTCTTTGGTCACTTTCCTGCT-3′
MyHC IIb	5′-GTGATTTCTCCTGTCACCTCTC-3′	5′-GGAGGACCGCAAGAACGTGCTGA-3′
β-Actin	5′-GTGGGCCGCTCTAGGCACCAA-3′	5′-CTCTTTGATGTCACGCACGATTTTC-3′

MyHC, myosin heavy chain; PGC-1α, peroxisome proliferator-activated receptor-γ coactivator-1α.

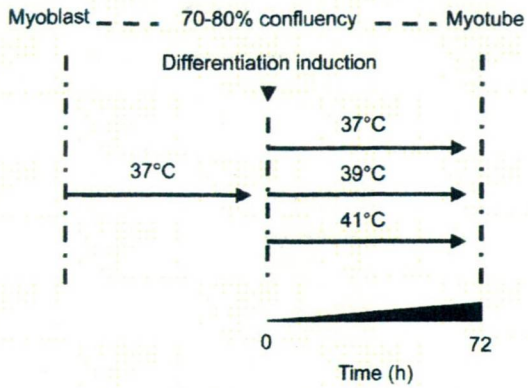

Fig. 1. Heat stress protocols. Cells were seeded in growth medium and incubated at 37°C. When they reached 70–80% confluency, the medium was changed to the differentiation-induction medium. At the same time, the culture temperature was set to 37, 39, or 41°C for 24–72 h.

ersham, UK). The membrane was then blocked in PBS containing 3% skim milk for 1 h and incubated with an appropriately diluted primary antibody and then for 1 h with a horseradish peroxidase-labeled secondary antibody. The immunoreactive bands were detected using an enhanced chemiluminescence kit (Amersham International). The chemiluminescent signal on the membrane was scanned using ChemiDoc XRS, Quantity One quantitation software (Bio-Rad). The band intensity was quantified using NIH Image. The housekeeping protein β-actin was used as an internal loading control for Western blot analysis.

Reverse Transcription-Polymerase Chain Reaction

Total mRNA from HSMM cells was isolated using RNeasy (Qiagen, Valencia, CA). After DNase treatment, cDNAs were obtained by reverse transcription of 2 μg of total RNA (Ready-to-Go T-primed first-strand kit; Amersham Biosciences, Piscataway, NJ). The primer sequences are listed in Table 1 (3, 6, 9, 18, 23, 50). The level of mRNA expression was determined by quantitative real-time reverse transcription-polymerase chain reaction (RT-PCR) in a fluorescent temperature cycler (ABI Prism 7000; Applied Biosystems, Darmstadt, Germany). The housekeeping gene β-actin was used as a control template for normalizing relative change of each mRNA in RT-PCR. Samples were incubated in the ABI Prism 7000 for an initial denaturation at 95°C for 10 min. Next, 40 PCR cycles were performed under the following conditions: 95°C for 15 s and 60°C for 1 min. SYBR green fluorescence (Power SYBR green PCR master mix; Applied Biosystems) emissions were determined after each cycle, and the synthesis of each gene mRNA was quantified using the ABI Prism 7000 SDS software (Applied Biosystems). The PCR was performed in triplicate.

Immunofluorescence

For immunofluorescent staining, cells incubated in petri dishes containing collagen type I-coated cover glasses at 37, 39, and 41°C for 24–72 h were washed with warm PBS at 37°C and fixed by incubation at room temperature in prewarmed (at 37°C) FME (4% formaldehyde, 2 mM $MgCl_2$, and 5 mM EGTA in PBS) for 10 min. Cells were washed three times with PBS and permeabilized with FME containing 0.3% Triton X-100 (FMET) for 10 min at room temperature. FMET-fixed cells were washed three times with PBS and kept in PBS containing 1% BSA and 0.02% sodium azide. Cells were immuno-

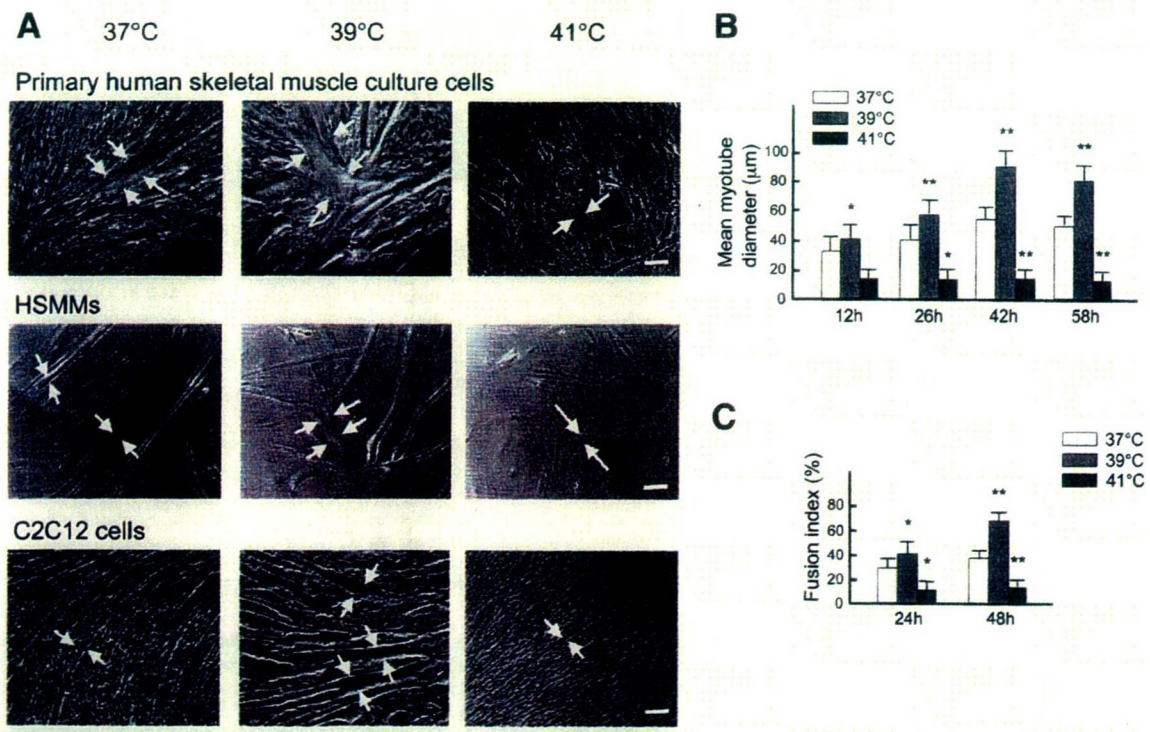

Fig. 2. Morphological changes of human and C2C12 myotubes after exposure to heat stress. *A*: representative images of myotubes in primary human skeletal muscle culture after 72-h exposure to heat stress, human skeletal muscle myoblasts (HSMMs) after 48-h exposure to heat stress, and C2C12 myotubes after 72-h exposure to heat stress. Arrows indicate edges of myotubes. Bars, 80 μm. *B*: changes in myotube diameter formed by C2C12 cells after exposure to heat stress. Each column shows the mean ± SD of 210 myotubes from 3 independent cultures. *C*: changes of fusion index of C2C12 cells after exposure to heat stress. Each column shows the mean ± SD of 3 independent cultures. ; $*P < 0.05$; $**P < 0.01$ compared with control (37°C).

histochemically stained with an appropriately diluted primary antibody and then for 1 h with a fluorescence-conjugated secondary antibody. The slides were then rinsed with PBS and mounting using 4,6-diamidino-2-phenylindole (DAPI). All photographs were viewed in a Nikon Eclipse TE 300 inverted microscope (Tokyo, Japan) and recorded with a digital camera (model 4742-95; Hamamatsu Photonics, Hamamatsu, Japan). Photographs were edited using Photoshop software (Adobe Photoshop version 7.0).

Measurement of Myotube Diameter and Fusion Index of C2C12 Cells

For each temperature condition, 7 different photomicrograph fields were randomly chosen from 3 independent cultures, and the width of the 10 largest myotubes in each field was measured. Mean values constituted a measure of 210 myotubes for each condition. The fusion index was defined as the ratio of the number of DAPI-stained nuclei in myotubes with three or more nuclei to the total number of DAPI-stained nuclei in each field. This percentage was determined by counting 1,000 nuclei per dish on three independent cultures for each condition.

Statistical Analysis

Data are means ± SD. Statistical significance ($P < 0.05$) between control cells incubated at 37°C and heat-stressed cells incubated at 39 or 41°C was determined by a one-way ANOVA followed by a Dunnett post hoc test.

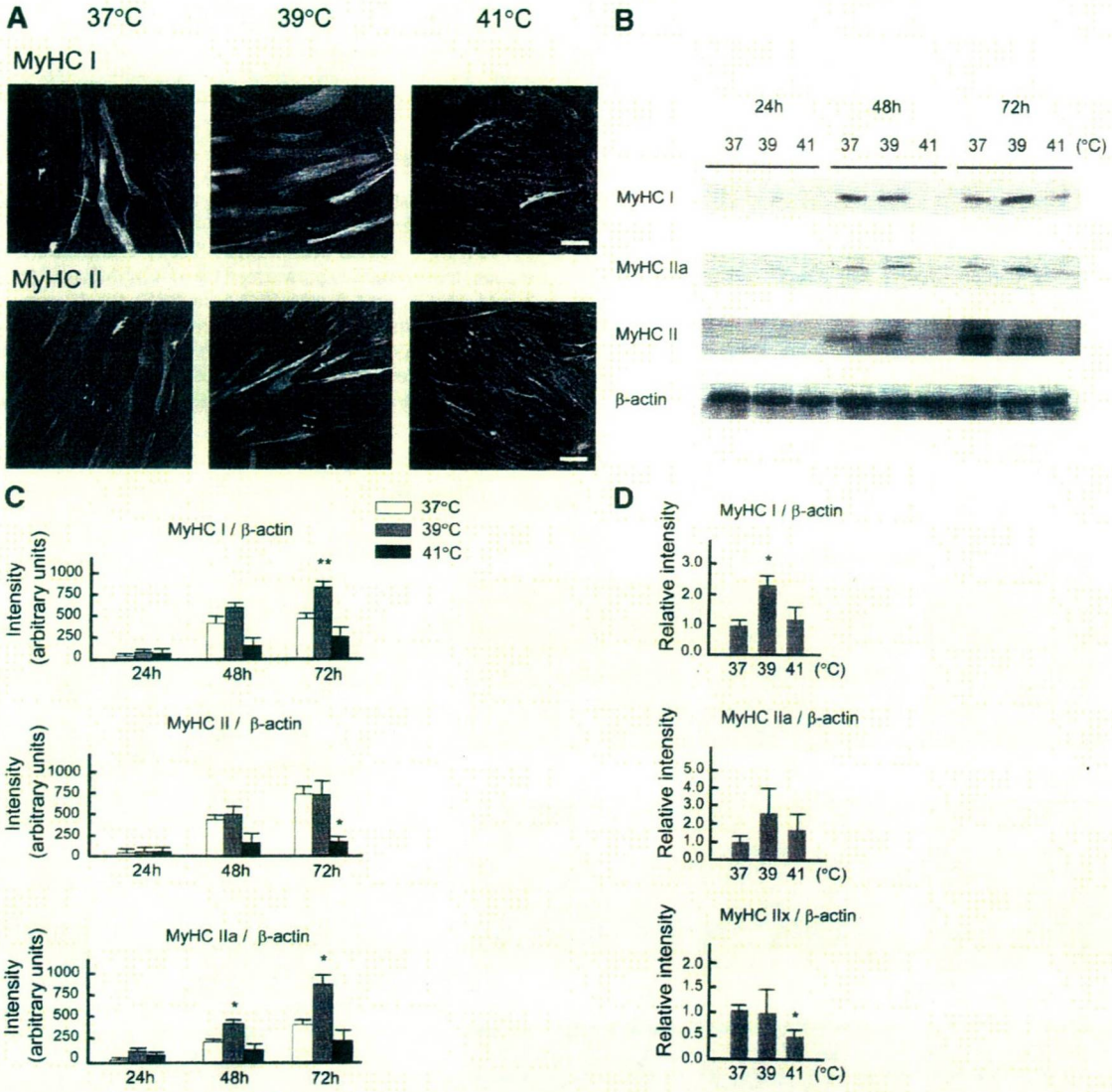

Fig. 3. Changes of myosin heavy chain (MyHC) isoform expression after heat stress treatment of HSMMs. *A*: representative fluorescent images of HSMMs after 72-h exposure to heat stress. MyHC types I and II were detected by immunofluorescence with the use of monoclonal antibodies against MyHC I (clone NOQ7.5.4D) and MyHC II (clone MY32) and secondary rhodamine-conjugated antibody. Bars, 80 μm. *B* and *C*: after exposure of HSMMs to heat stress for 24, 48, and 72 h, cells were harvested and subjected to Western blot analysis with antibodies against MyHC I (clone NOQ7.5.4D), II (clone MY32), and IIa (clone A4.74). MyHC II antibody recognized all the MyHC II isoforms. MyHC isoform expression was normalized to that of β-actin. Data show intensities relative to control (37°C). Data are means ± SD from 3 independent experiments with HSMMs from 3 different donors. *D*: after exposure of HSMMs to heat stress for 72 h, HSMMs were harvested. Total RNA was extracted and reverse transcribed. cDNA levels of MyHC isoform mRNAs in HSMMs were determined by RT-PCR and normalized to β-actin cDNA levels. Data show intensities relative to intensities of control (37°C). Data are means ± SD from 3 independent experiments with HSMMs from 3 different donors. $^{*}P < 0.05$; $^{**}P < 0.01$ compared with control (37°C).

RESULTS

Heat Stress Affects Myotube Formation

To investigate the direct effects of heat stress on myotube formation of cultured mammalian myoblasts, we incubated the cells at various temperatures in vitro, as shown in Fig. 1. Primary human skeletal muscle culture cells were exposed to various temperatures for 72 h. Myotubes incubated at 39°C showed an increased diameter compared with the control cells incubated at 37°C. The myotubes incubated at 41°C were poorly formed (Fig. 2*A*). To minimize the effects of contaminating fibroblasts in primary human skeletal muscle culture cells, we investigated whether a similar phenomenon (myotube enlargement) was observed in HSMMs. The results were consistent with that of the primary culture, with increased diameter when incubated at 39°C (Fig. 2*A*).

To test whether the phenomenon described above was also relevant to muscle cells of mice, we used C2C12 cells, which are of mice origin. As shown in Fig. 2, *A* and *B*, the diameter of the myotubes increased significantly after exposure to 39°C compared with the control cultures at 37°C; interestingly, there was no change in the diameter of the myotubes at 41°C.

Myotubes are formed by the fusion of singly nucleated myoblasts by differentiation-inducing stimuli. Hence, the enlargement of myotubes incubated at 39°C could be due to differences in the fusion process of myoblasts. To test this possibility, we measured the fusion index of C2C12 cells incubated at different temperatures. Compared with the control culture at 37°C, the fusion index was significantly increased at 39°C after 24 and 48 h of incubation, whereas the fusion index was significantly decreased at 41°C (Fig. 2*C*).

To identify temperature-dependent expression of HSPs after continuous heat stress, we analyzed the protein expression levels of a representative HSP (HSP70) by Western blot analysis of HSMMs extracts. In cells exposed to heat stress for 72 h, the protein level of HSP70 increased 2.7-fold at 39°C and 7.3-fold at 41°C compared with 37°C control (data not shown).

Heat exposure alters levels of MyHC isoforms in HSMMs and C2C12 cells

Since the function of skeletal muscle cells is highly linked to their structure, it is possible that the structural change, i.e., increased myotube diameter as described above, is accompanied by some functional changes in skeletal muscle cells. To test this possibility, we examined possible changes in MyHC isoforms in cells exposed to heat stress. Figure 3, *A* and *B*, shows representative immunostaining of HSMMs. The MyHC was targeted by either a primary antibody specific for MyHC I (NOQ7.5.4D) or an antibody specific for MyHC II (MY-32) (Fig. 3*A*). MY-32 recognized all MyHC II isoforms. These experiments indicated that HSMMs expressed both MyHC I and II. After exposure to heat stress for 72 h, HSMM myotubes expressing MyHC I at 39°C were larger in size compared with myotubes that were not heat-stressed. In contrast, HSMM myotubes expressing MyHC II at 39°C were of the same size compared with myotubes exposed to 37°C. The myotubes incubated at 41°C showed weak staining for both MyHC I and II.

In adult humans, there are three major MyHC isoforms (MyHC I and two subtypes of MyHC II, IIa and IIx) (12). Expression of MyHC I and II isoforms in HSMMs was confirmed by Western blot analysis and RT-PCR. We used β-actin as an internal control. There were no significant changes in the protein and mRNA levels of β-actin after heat stress in HSMMs (data not shown). To examine the protein levels of MyHC isoforms in HSMMs, we used MyHC I (NOQ7.5.4D), II (MY-32), and IIa (A4.74) (22) antibodies. As shown in Fig. 3, *B* and *C*, in HSMMs exposed to heat stress at 39°C, the protein levels of MyHC I increased after 72 h of incubation (1.6-fold, $P < 0.01$), whereas MyHC I protein levels were unaffected by heat stress at 41°C, compared with the control culture at 37°C. MyHC II antibody recognized both MyHC II isoforms. The total protein level of MyHC II did not change at 39°C after heat exposure but decreased at 41°C after 72 h ($P < 0.05$) compared with the 37°C control. In contrast, in cells exposed to heat stress at 39°C for 48 and 72 h, 1.8-fold ($P < 0.05$) and 2.1-fold increases ($P < 0.05$), respectively, were found in the levels of MyHC IIa protein compared with the 37°C control. Those results implied that MyHC IIx expression decreased after exposure to heat stress at 39°C. We also

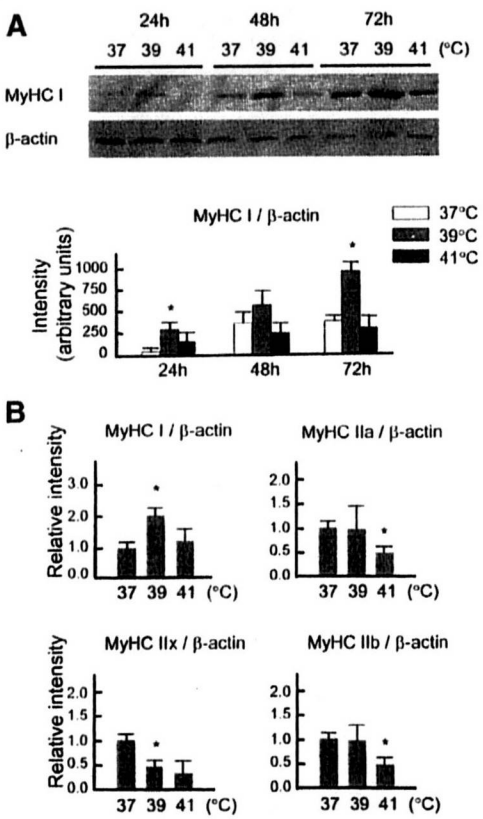

Fig. 4. Changes of MyHC isoform expression after heat stress treatment of C2C12 cells. *A*: after exposure of C2C12 cells to heat stress for 24, 48, and 72 h, cells were harvested and subjected to Western blot analysis with an antibody against MyHC type I. MyHC type I expression was normalized to β-actin. Data show intensities relative to control (37°C). Data are means ± SD from 3 independent cell cultures. *B*: after exposure of C2C12 cells to heat stress for 72 h, C2C12 cells were harvested. Total RNA was extracted and reverse transcribed. cDNA levels of MyHC isoform mRNAs in C2C12 cells were determined by RT-PCR and normalized to β-actin cDNA levels. Data show intensities relative to intensities of control (37°C). Data are means ± SD from 3 independent cell cultures. $*P < 0.05$; $**P < 0.01$ compared with control (37°C).

examined corresponding changes in the mRNA levels of MyHC isoforms in HSMMs. As shown in Fig. 3*D*, in HSMMs exposed to heat stress at 39°C for 72 h, the mRNA levels of MyHC I increased 2.3-fold compared with cells that were not heat-stressed ($P < 0.05$), whereas the mRNA levels of MyHC IIa tended to increase when cells were exposed to 39°C ($P = 0.23$). In contrast, the mRNA levels of MyHC IIx in cells exposed to 41°C decreased 47% compared with cells that were not heat-stressed ($P < 0.05$). These data indicated that incubation of cells at 39°C induced differentiation, leading to a fast-to-slow fiber-type shift in HSMMs.

In small mammals, there are four major MyHC isoforms in skeletal muscle fibers: MyHC I and three subtypes of MyHC II, IIa, IIx, and IIb (39). Expression of MyHC I and II isoforms in C2C12 cells was confirmed by Western blot analysis and RT-PCR. We used β-actin as an internal control. There were no significant changes in the protein and mRNA levels of β-actin after heat stress in C2C12 cells (data not shown). To examine the protein expression of MyHC I in C2C12 cells, we used an antibody targeted against MyHC I (NOQ7.5.4D). In cells exposed to 39°C, the protein level of MyHC I increased after 24 (4.8-fold, $P < 0.05$) and 72 h (2.4-fold, $P < 0.05$) of incubation compared with cells that were not heat-stressed (Fig. 4*A*). We examined changes in expression of MyHC I and II isoforms in C2C12 cells by using RT-PCR. As shown in Fig. 4*B*, in C2C12 cells exposed to heat stress at 39°C for 72 h, the mRNA levels of MyHC I increased 2.0-fold compared with cells that were not heat-stressed ($P < 0.05$), whereas the mRNA levels of MyHC IIx in cells exposed to 39°C decreased 45% compared with cells that were not heat-stressed ($P < 0.05$). These data indicated that incubation of cells at 39°C induced differentiation, leading to a fast-to-slow fiber-type shift in C2C12 cells.

Heat Exposure Alters Levels of MRFs in HSMMs and C2C12 Cells

MRFs, which include MyoD and myogenin, are expressed in skeletal muscle, with each MRF playing a crucial role in muscle cell specification and differentiation (44). MyoD mRNA was shown to be most prevalent in fast glycolytic muscles, whereas myogenin mRNA was shown to be most prevalent in slow oxidative muscles (15). To test the possible involvement of MRFs in the myotube enlargement and the fiber-type shift in heat-stressed cells, we next addressed the protein levels of MyoD and myogenin in both types of cells after a 72-h exposure to heat stress. The level of myogenin was enhanced in the 39°C culture ($P < 0.05$) relative to that at 37°C, but no significant change in the levels of MyoD was detected after heat stress in HSMMs (Fig. 5*A*). We further tested whether there were any changes in the levels of MyoD and myogenin in C2C12 cells after heat stress. In cells exposed to heat stress for 72 h, the protein levels of MyoD decreased at 39 ($P < 0.05$) and 41°C ($P < 0.01$), whereas the protein levels of myogenin increased at 39°C ($P < 0.01$), compared with cells that were not exposed to heat stress (Fig. 5*B*). Figure 5*C* shows representative immunostaining for myogenin in C2C12 cells. Large myotubes at 39°C contained more myogenin-positive nuclei than did myotubes at 37°C. These data suggested that incubation of cells at 39°C induced myogenin expression, which enhanced myoblast fusion.

Heat Exposure Alters PGC-1α Protein Expression in HSMMs and C2C12 Cells

PGC-1α is one of the factors regulating muscle fiber-type determination (21). To determine any changes in expression of PGC-1α after exposure of cells to heat stress, we examined the protein level of PGC-1α in C2C12 cells after heat stress. In cells exposed to 39°C, the protein level of PGC-1α increased after 48 ($P < 0.05$) and 72 h ($P < 0.01$) of incubation compared with cells that were not heat-stressed (Fig. 6*A*). When we examined the protein level of PGC-1α in HSMMs by Western blot analysis, it could not be detected at any point in time (24, 48, and 72 h). Thus we determined PGC-1α expression in HSMMs by RT-PCR. After heat stress for 24 h, the mRNA level of PGC-1α was enhanced in the 39°C culture

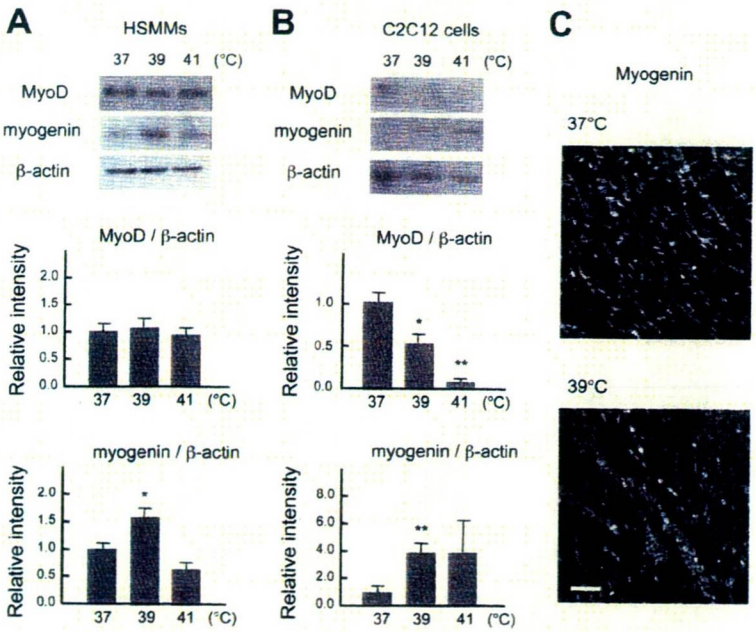

Fig. 5. Changes in the levels of MyoD and myogenin after heat stress treatment of HSMMs and C2C12 cells. *A* and *B*: After exposure to heat stress for 72 h, cells were harvested and subjected to Western blot analysis with antibodies against MyoD and myogenin. Expression of MyoD and myogenin was normalized to β-actin. Data show intensities relative to intensities of control (37°C). Data are means ± SD from 3 independent experiments with HSMMs from 3 different donors (*A*) or 3 C2C12 cell cultures (*B*). *$P < 0.05$; **$P < 0.01$ compared with control (37°C). *C*: representative fluorescent images of C2C12 cells after 72-h exposure to heat stress. Myogenin was detected by immunofluorescence with the use of monoclonal anti-myogenin antibody (F5D) and secondary rhodamine-conjugated antibody. Bars, 80 μm.

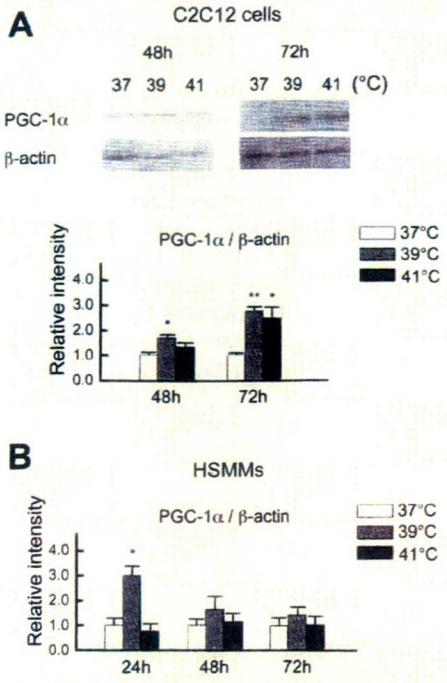

Fig. 6. Changes of the levels of peroxisome proliferator-activated receptor-γ coactivator-1α (PGC-1α) after heat stress in C2C12 cells and HSMMs. *A*: after exposure of C2C12 cells to heat stress for 48 and 72 h, cells were harvested and subjected to Western blot analysis with an antibody against PGC-1α. PGC-1α expression was normalized to β-actin. Data express intensities relative to control (37°C). Data are means ± SD from 3 independent cell cultures. *B*: after exposure of HSMMs to heat stress for 24, 48, and 72 h, HSMMs were harvested. Total RNA was extracted and reverse transcribed. cDNA levels of MyHC isoform mRNAs in HSMMs were determined by RT-PCR and normalized to β-actin cDNA levels. Data show intensities relative to control (37°C). Data are means ± SD from 3 independent experiments with HSMMs from 3 different donors. $*P < 0.05$; $**P < 0.01$ compared with each control (37°C).

($P < 0.05$) relative to that at 37°C, but no significant change in the mRNA levels of PGC-1α was detected after heat stress for 48 and 72 h in HSMMs (Fig. 6*B*).

Several studies have shown that MAPKs are involved in the determination of muscle fiber type phenotypes (27, 31). It is possible that heat stress affected the phosphorylation of ERK1/2 or p38 MAPK. ERK1/2 is activated by short- and long-term low-frequency electrical stimulation, which involved fast-to-slow fiber-type conversion (2, 31). Thus we next measured the phosphorylation states of ERK1/2 and p38 MAPK in HSMMs and C2C12 cells after heat stress for 1, 24, and 48 h. The relative amounts of phosphorylated forms of both ERK1/2 and p38 MAPK did not change at any point in time in either type of cells (data not shown).

DISCUSSION

We defined incubation at 39°C as continuous mild heat stress (CMHS) and 41°C as continuous severe heat stress (CSHS). Our analysis revealed that CMHS enhanced myotube diameter of primary human skeletal muscle culture cells, HSMMs, and C2C12 cells. In contrast, during CSHS, myotubes were poorly formed. In HSMMs and C2C12 cells exposed to CMHS, the mRNA and protein levels of MyHC type I was increased compared with the control cultures. The mRNA level of MyHC IIx was unaltered in HSMMs and decreased in C2C12 cells compared with cells that were not exposed to heat stress. These results indicate that CMHS induced the differentiation of the cells, causing a fast-to-slow fiber-type shift in C2C12 cells and HSMMs. Our results also showed upregulated myogenin expression after CMHS. We next examined upstream signals that might be responsible for the fiber-type shift. CMHS enhanced mRNA and protein levels of PGC-1α in HSMMs and C2C12 cells.

The effects of heat stress on cellular function are pleiotropic. These include denaturation and disaggregation of proteins, cytoskeletal disruption, cell cycle inhibition, and changes in membrane permeability (20). Heat stress induces HSP70, which plays a role in maintaining protein homeostasis, a fine balance among protein synthesis, protein degradation, and protein refolding (38, 51). In addition, detection of HSPs is an indication of the formation of denatured protein and the presence of thermal damage (20). In our study, the levels of HSP70 were upregulated with increased temperature after heat stress. Since myogenic differentiation was not inhibited during CMHS, the amount of protein denaturation may be low. In contrast, CSHS inhibited myotube formation. CSHS might increase the amount of denatured and aggregated proteins and disrupt protein homeostasis, which might in turn lead to intracellular dysfunction.

The fast-to-slow shift in MyHC isoform expression can be induced under several conditions. Strength training led to a shift in MyHC isoform composition from MyHC IIx to IIa in human triceps brachii (23). Chronic low-frequency electrical stimulation (CLFS) increases the expression of MyHC I or IIa, whereas it decreases that of MyHC IIx or IIb in human and rat tibialis anterior (26, 47). So far, changes of MyHC following heat stress have not been reported. Our study is the first to report that CMHS induced differentiation and a fast-to-slow fiber-type shift of myoblasts in two different species. These observations might be a general characteristic of mammalian myoblasts.

Several signaling pathways regulate skeletal muscle fiber-type shift. Murgia et al. (31) suggested that the Ras-ERK pathway was required for reestablishment of the slow fiber program in a model simulating nerve impulse activity. p38 MAPK has been reported to control MyHC IIx promoter activity in myotubes (27). Our study demonstrated that CMHS did not enhance the activity of either ERK1/2 or p38 MAPK. Another investigator suggested that the ERK1/2 pathway played an important role in the maintenance of fast-twitch fiber phenotype (41). So far, the role of MAPK signaling cascades in modulating muscle fiber type remains unclear.

Transgenic expression of PGC-1α in fast-twitch glycolytic muscles promotes mitochondrial biogenesis and oxidative metabolism and transforms the type IIb muscle fibers into a more oxidative phenotype (21). Therefore, PGC-1α might be the principal factor regulating muscle fiber-type determination. AMP-activated protein kinase (AMPK), calcineurin, CaMK, and p38 MAPK pathways have been implicated in the regulation of PGC-1α expression and activity (8). Since the activation of p38 MAPK did not change, the expression of PGC-1α induced by CMHS in the present study might be attributable to other pathways. Calcium is thought to be involved in the upstream signaling of PGC-1α for several reasons. Calcium activates calcineurin and CaMK, which regulate the expression

of PGC-1α (8, 48). Kubis et al. (17) reported that a modest but sustained rise in intracellular free Ca^{2+} concentration ($[Ca^{2+}]_i$) caused by low concentrations of the Ca^{2+} ionophore A-23187 in the culture medium induced fast-to-slow fiber-type conversion in rabbit primary skeletal muscle cells. With regard to heat stress and Ca^{2+} homeostasis, heat stress is known to increase $[Ca^{2+}]_i$ (5, 28). Recent evidence suggests that exposure of mammalian skeletal muscle to temperatures in the range of 40–43°C for 30 min reduced the ability of the sarcoplasmic reticulum to accumulate Ca^{2+} (46). Accordingly, CMHS may induce changes in Ca^{2+} homeostasis, which could lead to the fiber-type shift through the PGC-1α pathway in myoblasts.

In the present study, CMHS enhanced the level of expression of myogenin protein, whereas there was no increase in the level of MyoD. CMHS enhanced myoblast fusion and myotube diameter of C2C12 cells and HSMMs. Myogenin is required to initiate terminal differentiation and fusion (1, 25). These results indicated that myogenin played a role in CMHS-enhanced myogenic differentiation. It has been reported that MyoD is prevalent in fast-twitch muscles and myogenin in slow-twitch muscles (15). Several lines of evidence have implicated myogenin in the fast-to-slow fiber-type shift (7, 15, 26, 37, 47). In cultured myotubes, a moderate increase in $[Ca^{2+}]_i$ induced a fast-to-slow fiber-type shift and enhanced the protein expression level of myogenin but not other myogenic factors (45). In the fast-twitch muscle of hypothyroid rats, shifting to a slow direction by CLFS increased the expression of myogenin with unaltered MyoD levels (37). Hughes et al. (14) reported that the overexpression of myogenin in skeletal muscles of transgenic mice influenced the activity of metabolic enzymes, inducing a shift from glycolytic metabolism to oxidative metabolism. In their study, no change in fiber type-specific MyHC isoform expression was observed. Furthermore, Schluter and Fitts (40) reported that oxidative enzyme activity and MyHC type were independently regulated in rat skeletal muscle. Thus it appears that myogenin plays a role in metabolic adaptation to a fast-to-slow fiber-type shift, although no study has demonstrated the link between myogenin expression and mild changes in temperature.

The results of this study showed that CMHS increased the fusion index, myotube diameter, and fast-to-slow fiber-type shift, whereas CSHS did not promote myotube formation. The beneficial effect of low doses of a stressful agent, which is otherwise toxic at high doses, is known as hormesis (24). Although local hyperthermia is used to promote blood flow and enhance healing after muscle injuries (19), the mechanism by which this occurs has not been fully elucidated. During hyperthermia, temperature in skeletal muscle ranges from 36 to 44°C (4, 19). On skeletal muscle injury, satellite cells are released and activated to become myoblasts, which eventually differentiate into myotubes and mature muscle fibers (13). We observed the effects of temperature on the in vitro differentiation of myoblasts and have elucidated a possible mechanism of heat stress. We postulate that local hyperthermia increases muscle temperature and thereby promotes myogenic differentiation and fast-to-slow muscle fiber-type shift in vivo.

There is increasing evidence suggesting that mitochondrial dysfunction in skeletal muscle is involved in insulin resistance and type 2 diabetes (16). PGC-1α promotes mitochondrial biogenesis and slow fiber formation in skeletal muscle (21). Two studies have reported that decreases in the amount of PGC-1α in skeletal muscle are associated with human type 2 diabetes and an increased risk of developing type 2 diabetes (29, 34). Taking these findings together, PGC-1α appears to play a role in disorders such as insulin resistance and diabetes. Also, several lines of evidence demonstrate that both short-term exercise and endurance training activate PGC-1α expression in skeletal muscle (8, 36). Pilegaard et al. (36) reported that exercise induces a dramatic transient increase in PGC-1α transcription and mRNA content, peaking within 2 h after exercise in human skeletal muscle. Our observations of PGC-1α mRNA expression in HSMMs were similar to that reported by Pilegaard (36). It is possible that a mild increase in temperature due to exercise causes PGC-1α expression. Further studies of CMHS should provide insight into prevention of diseases involving mitochondrial dysfunction and identify factors that induce PGC-1α following exercise.

ACKNOWLEDGMENTS

We thank Dr. Kiyoshi Kikumoto for providing human skeletal muscle samples. We also thank Drs. Takashi Sakurai and Shunichiro Kubota for generous support of our research. We are grateful to Dr. Ryoichi Matsuda for kindly providing antibodies.

REFERENCES

1. **Andres V, Walsh K.** Myogenin expression, cell cycle withdrawal, and phenotypic differentiation are temporally separable events that precede cell fusion upon myogenesis. *J Cell Biol* 132: 657–666, 1996.
2. **Aronson D, Dufresne SD, Goodyear LJ.** Contractile activity stimulates the c-Jun NH_2-terminal kinase pathway in rat skeletal muscle. *J Biol Chem* 272: 25636–25640, 1997.
3. **Balagopal P, Olney R, Darmaun D, Mougey E, Dokler M, Sleck G, Hammond D.** Oxandrolone enhances skeletal muscle myosin synthesis and alters global gene expression profile in Duchenne muscular dystrophy. *Am J Physiol Endocrinol Metab* 290: E530–E539, 2006.
4. **Borrell RM, Parker R, Henley EJ, Masley D, Repinecz M.** Comparison of in vivo temperatures produced by hydrotherapy, paraffin wax treatment, and Fluidotherapy. *Phys Ther* 60: 1273–1276, 1980.
5. **Calderwood SK, Stevenson MA, Hahn GM.** Effects of heat on cell calcium and inositol lipid metabolism. *Radiat Res* 113: 414–425, 1988.
6. **Casas F, Pessemesse L, Grandemange S, Seyer P, Gueguen N, Baris O, Lepourry L, Cabello G, Wrutniak-Cabello C.** Overexpression of the mitochondrial T3 receptor p43 induces a shift in skeletal muscle fiber types. *PLoS One* 3: e2501, 2008.
7. **Ekmark M, Gronevik E, Schjerling P, Gundersen K.** Myogenin induces higher oxidative capacity in pre-existing mouse muscle fibres after somatic DNA transfer. *J Physiol* 548: 259–269, 2003.
8. **Finck BN, Kelly DP.** PGC-1 coactivators: inducible regulators of energy metabolism in health and disease. *J Clin Invest* 116: 615–622, 2006.
9. **Frederiksen CM, Hojlund K, Hansen L, Oakeley EJ, Hemmings B, Abdallah BM, Brusgaard K, Beck-Nielsen H, Gaster M.** Transcriptional profiling of myotubes from patients with type 2 diabetes: no evidence for a primary defect in oxidative phosphorylation genes. *Diabetologia* 51: 2068–2077, 2008.
10. **Gaster M, Beck-Nielsen H, Schroder HD.** Proliferation conditions for human satellite cells. The fractional content of satellite cells. *APMIS* 109: 726–734, 2001.
11. **Hanson DF.** Fever, temperature, and the immune response. *Ann NY Acad Sci* 813: 453–464, 1997.
12. **Hilber K, Galler S, Gohlsch B, Pette D.** Kinetic properties of myosin heavy chain isoforms in single fibers from human skeletal muscle. *FEBS Lett* 455: 267–270, 1999.
13. **Huard J, Li Y, Fu FH.** Muscle injuries and repair: current trends in research. *J Bone Joint Surg Am* 84-A: 822–832, 2002.
14. **Hughes SM, Chi MM, Lowry OH, Gundersen K.** Myogenin induces a shift of enzyme activity from glycolytic to oxidative metabolism in muscles of transgenic mice. *J Cell Biol* 145: 633–642, 1999.
15. **Hughes SM, Taylor JM, Tapscott SJ, Gurley CM, Carter WJ, Peterson CA.** Selective accumulation of MyoD and myogenin mRNAs in fast and slow adult skeletal muscle is controlled by innervation and hormones. *Development* 118: 1137–1147, 1993.

16. **Kelley DE, He J, Menshikova EV, Ritov VB.** Dysfunction of mitochondria in human skeletal muscle in type 2 diabetes. *Diabetes* 51: 2944–2950, 2002.
17. **Kubis HP, Haller EA, Wetzel P, Gros G.** Adult fast myosin pattern and Cu^{2+}-induced slow myosin pattern in primary skeletal muscle culture. *Proc Natl Acad Sci USA* 94: 4205–4210, 1997.
18. **Lamba DA, Karl MO, Ware CB, Reh TA.** Efficient generation of retinal progenitor cells from human embryonic stem cells. *Proc Natl Acad Sci USA* 103: 12769–12774, 2006.
19. **Lehmann JF, de Lateur BJ.** Diathermy and superficial heat, laser and cold therapy. In: *Krusen's Handbook of Physical Medicine and Rehabilitation*, edited by Kottke FJ and Lehmann JF. Philadelphia, PA: Saunders, 1990. p. 283–435.
20. **Lepock JR.** Cellular effects of hyperthermia: relevance to the minimum dose for thermal damage. *Int J Hyperthermia* 19: 252–266, 2003.
21. **Lin J, Wu H, Tarr PT, Zhang CY, Wu Z, Boss O, Michael LF, Puigserver P, Isotani E, Olson EN, Lowell BB, Bassel-Duby R, Spiegelman BM.** Transcriptional co-activator PGC-1 alpha drives the formation of slow-twitch muscle fibres. *Nature* 418: 797–801, 2002.
22. **Liu JX, Thornell LE, Pedrosa-Domellof F.** Muscle spindles in the deep muscles of the human neck: a morphological and immunocytochemical study. *J Histochem Cytochem* 51: 175–186, 2003.
23. **Liu Y, Schlumberger A, Wirth K, Schmidtbleicher D, Steinacker JM.** Different effects on human skeletal myosin heavy chain isoform expression: strength vs. combination training. *J Appl Physiol* 94: 2282–2288, 2003.
24. **Luckey T.** *Hormesis with Ionizing Radiation*. Boca Raton, FL: CRC, 1980.
25. **Ludolph DC, Konieczny SF.** Transcription factor families: muscling in on the myogenic program. *FASEB J* 9: 1595–1604, 1995.
26. **Martins KJ, Gordon T, Pette D, Dixon WT, Foxcroft GR, Maclean IM, Putman CT.** Effect of satellite cell ablation on low-frequency-stimulated fast-to-slow fibre-type transitions in rat skeletal muscle. *J Physiol* 572: 281–294, 2006.
27. **Meissner JD, Chang KC, Kubis HP, Nebreda AR, Gros G, Scheibe RJ.** The p38alpha/beta mitogen-activated protein kinases mediate recruitment of CREB-binding protein to preserve fast myosin heavy chain IId/x gene activity in myotubes. *J Biol Chem* 282: 7265–7275, 2007.
28. **Mikkelsen RB, Reinlib L, Donowitz M, Zahniser D.** Hyperthermia effects on cytosolic $[Ca^{2+}]$: analysis at the single cell level by digitized imaging microscopy and cell survival. *Cancer Res* 51: 359–364, 1991.
29. **Mootha VK, Lindgren CM, Eriksson KF, Subramanian A, Sihag S, Lehar J, Puigserver P, Carlsson E, Ridderstrale M, Laurila E, Houstis N, Daly MJ, Patterson N, Mesirov JP, Golub TR, Tamayo P, Spiegelman B, Lander ES, Hirschhorn JN, Altshuler D, Groop LC.** PGC-1alpha-responsive genes involved in oxidative phosphorylation are coordinately downregulated in human diabetes. *Nat Genet* 34: 267–273, 2003.
30. **Moyer HR, Delman KA.** The role of hyperthermia in optimizing tumor response to regional therapy. *Int J Hyperthermia* 24: 251–261, 2008.
31. **Murgia M, Serrano AL, Calabria E, Pallafacchina G, Lomo T, Schiaffino S.** Ras is involved in nerve-activity-dependent regulation of muscle genes. *Nat Cell Biol* 2: 142–147, 2000.
32. **Naya FJ, Mercer B, Shelton J, Richardson JA, Williams RS, Olson EN.** Stimulation of slow skeletal muscle fiber gene expression by calcineurin in vivo. *J Biol Chem* 275: 4545–4548, 2000.
33. **Park HG, Han SI, Oh SY, Kang HS.** Cellular responses to mild heat stress. *Cell Mol Life Sci* 62: 10–23, 2005.
34. **Patti ME, Butte AJ, Crunkhorn S, Cusi K, Berria R, Kashyap S, Miyazaki Y, Kohane I, Costello M, Saccone R, Landaker EJ, Goldfine AB, Mun E, DeFronzo R, Finlayson J, Kahn CR, Mandarino LJ.** Coordinated reduction of genes of oxidative metabolism in humans with insulin resistance and diabetes: potential role of PGC1 and NRF1. *Proc Natl Acad Sci USA* 100: 8466–8471, 2003.
35. **Pette D, Staron RS.** Myosin isoforms, muscle fiber types, and transitions. *Microsc Res Tech* 50: 500–509, 2000.
36. **Pilegaard H, Saltin B, Neufer PD.** Exercise induces transient transcriptional activation of the PGC-1alpha gene in human skeletal muscle. *J Physiol* 546: 851–858, 2003.
37. **Putman CT, Dusterhoft S, Pette D.** Satellite cell proliferation in low frequency-stimulated fast muscle of hypothyroid rat. *Am J Physiol Cell Physiol* 279: C682–C690, 2000.
38. **Rokutan K, Hirakawa T, Teshima S, Nakano Y, Miyoshi M, Kawai T, Konda E, Morinaga H, Nikawa T, Kishi K.** Implications of heat shock/stress proteins for medicine and disease. *J Med Invest* 44: 137–147, 1998.
39. **Schiaffino S, Reggiani C.** Myosin isoforms in mammalian skeletal muscle. *J Appl Physiol* 77: 493–501, 1994.
40. **Schluter JM, Fitts RH.** Shortening velocity and ATPase activity of rat skeletal muscle fibers: effects of endurance exercise training. *Am J Physiol Cell Physiol* 266: C1699–C1713, 1994.
41. **Shi H, Scheffler JM, Pleitner JM, Zeng C, Park S, Hannon KM, Grant AL, Gerrard DE.** Modulation of skeletal muscle fiber type by mitogen-activated protein kinase signaling. *FASEB J* 22: 2990–3000, 2008.
42. **Shui C, Scutt A.** Mild heat shock induces proliferation, alkaline phosphatase activity, and mineralization in human bone marrow stromal cells and Mg-63 cells in vitro. *J Bone Miner Res* 16: 731–741, 2001.
43. **Smith W.** The application of cold and heat in the treatment of athletic injuries. In: *Thermal Agents in Rehabilitation*, edited by Michlovitz SL. Philadelphia, PA: Davis, 1990. p. 245–256.
44. **Tapscott SJ.** The circuitry of a master switch: MyoD and the regulation of skeletal muscle gene transcription. *Development* 132: 2685–2695, 2005.
45. **Thelen MH, Simonides WS, Muller A, van Hardeveld C.** Cross-talk between transcriptional regulation by thyroid hormone and myogenin: new aspects of the Ca^{2+}-dependent expression of the fast-type sarcoplasmic reticulum Ca^{2+}-ATPase. *Biochem J* 329: 131–136, 1998.
46. **van der Poel C, Stephenson DG.** Effects of elevated physiological temperatures on sarcoplasmic reticulum function in mechanically skinned muscle fibers of the rat. *Am J Physiol Cell Physiol* 293: C133–C141, 2007.
47. **Vissing K, Andersen JL, Harridge SD, Sandri C, Hartkopp A, Kjaer M, Schjerling P.** Gene expression of myogenic factors and phenotype-specific markers in electrically stimulated muscle of paraplegics. *J Appl Physiol* 99: 164–172, 2005.
48. **Wu H, Kanatous SB, Thurmond FA, Gallardo T, Isotani E, Bassel-Duby R, Williams RS.** Regulation of mitochondrial biogenesis in skeletal muscle by CaMK. *Science* 296: 349–352, 2002.
49. **Wust P, Gellermann J, Rau B, Loffel J, Speidel A, Stahl H, Riess H, Vogl TJ, Felix R, Schlag PM.** Hyperthermia in the multimodal therapy of advanced rectal carcinomas. *Recent Results Cancer Res* 142: 281–309, 1996.
50. **Xu X, Zhang W, Kone BC.** CREB trans-activates the murine H^+-K^+-ATPase α_2-subunit gene. *Am J Physiol Cell Physiol* 287: C903–C911, 2004.
51. **Yamaguchi T, Arai H, Katayama N, Ishikawa T, Kikumoto K, Atomi Y.** Age-related increase of insoluble, phosphorylated small heat shock proteins in human skeletal muscle. *J Gerontol A Biol Sci Med Sci* 62: 481–489, 2007.

research articles Journal of proteome research

Identification of Glycoproteins Carrying a Target Glycan-Motif by Liquid Chromatography/Multiple-Stage Mass Spectrometry: Identification of Lewis x-Conjugated Glycoproteins in Mouse Kidney

Noritaka Hashii,[†,‡] Nana Kawasaki,*[,†,‡] Satsuki Itoh,[†] Yukari Nakajima,[†,‡] Akira Harazono,[†] Toru Kawanishi,[§] and Teruhide Yamaguchi[†]

Division of Biological Chemistry and Biologicals, National Institute of Health Sciences, 1-18-1 Kamiyouga, Setagaya-ku, Tokyo 158-8501, Japan, and Core Research for Evolutional Science and Technology (CREST) of the Japan Science and Technology Agency (JST), 4-1-8 Hon-cho, Kawaguchi, Saitama 332-0012 Japan

Received January 20, 2009

Certain glycan motifs in glycoproteins are involved in several biological events and diseases. To understand the roles of these motifs, a method is needed to identify the glycoproteins that carry them. We previously demonstrated that liquid chromatography−multiple-stage mass spectrometry (LC−MS^n) allowed for differentiation of oligosaccharides attached to Lewis-motifs, such as Lewis x (Le^x, Galβ1−4(Fucα1−3)GlcNAc) from other glycans. We successfully discriminated Le^x-conjugated oligosaccharides from other N-linked oligosaccharides derived from mouse kidney proteins by using Lewis-motif-distinctive ions, a deoxyhexose (dHex) + hexose (Hex) + *N*-acetylhexsosamine (HexNAc) fragment (*m/z* 512), and a Hex + HexNAc fragment (*m/z* 366). In the present study, we demonstrated that this method could be used to identify the Le^x-conjugated glycoproteins. All proteins in the mouse kidney were digested into peptides, and the fucosylated glycopeptides were enriched by lectin-affinity chromatography. The resulting fucosylated glycopeptides were subjected to two different runs of LC−MS^n using a Fourier- transform ion cyclotron resonance mass spectrometer (FTICR−MS) and an ion trap-type mass spectrometer. After the first run, we picked out product ion spectra of the expected Le^x-conjugated glycopeptides based on the presence of Lewis-motif-distinctive ions and assigned a peptide + HexNAc or peptide + (dHex)HexNAc fragment in each spectrum. Then the fucosylated glycopeptides were subjected to a second run in which the peptide-related fragments were set as precursor ions. We successfully identified γ-glutamyl transpeptidase 1 (γ-GTP1), low-density lipoprotein receptor-related protein 2 (LRP2), and a cubilin precursor as Le^x-conjugated glycoproteins by sequencing of 2−5 glycopeptides. In addition, it was deduced that cadherin 16, dipeptidase I, H-2 class I histocompatibility antigen, K−K alpha precursor (H2−K(k)), and alanyl (membrane) aminopeptidase could be Le^x-conjugated glycoproteins from the good agreement between the experimental and theoretical masses and fragment patterns. The results indicated that our method could be applicable for the identification and screening of glycoproteins carrying target glycan-motifs, such as Lewis epitopes.

Keywords: liquid chromatography/multiple-stage mass spectrometry • specific detection • database search analysis • Lewis x-conjugated oligosaccharides

Introduction

Glycosylation is one of the most common post-translational modifications of proteins.[1,2] Certain glycan motifs on glycoproteins are involved in several biological events, including cell adhesion,[3] differentiation and development. They are also known to be closely associated with some diseases, such as tumors and hepatic diseases.[4−6] Glycomics, the study of all glycoconjugates in a cell type or in an organism, is crucial to understanding the mechanisms of glycan-mediated biological events and diseases.[7,8] Mass spectrometry (MS) and multiple-stage mass spectrometry (MS^n) in combination with several types of chromatography are known to be the most powerful tools of structural glycomics.[9−14] There are two major approaches to mass spectrometric glycome analysis. One is mass spectrometric glycan profiling, which is achieved by online or off-line liquid chromatography/mass spectrometry (LC−MS) of oligosaccharides enzymatically or chemically released from proteins.[15−22] This technique has advantages for conducting a detailed structural analysis and a quantitative analysis of

* To whom correspondence should be addressed. Division of Biological Chemistry and Biologicals, National Institute of Health Sciences, 1-18-1 Kamiyouga, Setagaya-ku, Tokyo 158-8501, Japan. Fax: +81-3-3700-9084. E-mail: nana@nihs.go.jp.
† National Institute of Health Sciences.
‡ Japan Science and Technology Agency.
§ Division of Drugs, National Institute of Health Sciences.

10.1021/pr9000527 CCC: $40.75

oligosaccharides,[23-25] but it does not provide any information on protein sources that carry the glycans of interest. The other approach is the mass spectrometric mapping of proteolytic digests. This method enables us to characterize glycan structures based on fragment ions,[26-31] and to deduce the peptide sequence from b- and y-ions that arise from the peptide backbone.[27] In addition to these approaches, glycomics require more advanced methods that can identify target proteins carrying a glycan motif of interest; that is to say, a technique for focused glycomics.

Lectin and immunological-based approaches have been widely used for the specific detection of target glycans and glycoproteins.[32-34] There have been numerous reports on the use of MS in combination with affinity chromatography and Western blotting with lectins or glyco-epitope-specific antibodies.[35-38] In a previous study, we demonstrated that LC−MS^n is also useful for the analysis of target glycans in a complex mixture.[39] Several glycan motifs often yield motif-specific ions by MS^n, along with common glycan-related ions such as the *N*-acetylhexosamine (HexNAc) fragment (*m/z* 204) and hexose (Hex) + HexNAc fragment (*m/z* 366).[40,41] For example, Lewis-motifs that consist of fucose (Fuc), galactose (Gal) and *N*-acetylglucosamine (GlcNAc) yield a distinctive ion at *m/z* 512 that corresponds to the B-type ion of deoxyhexose (dHex) + Hex + HexNAc. This B-type ion subsequently provides the product ion at *m/z* 366 ([Hex + HexNAc|$^+$) by MS/MS/MS. Using these Lewis-motif-distinctive ions, we successfully differentiated the oligosaccharides bearing the Lewis-motifs from many other oligosaccharides in mouse kidneys.[39] This method could be used to differentiate the Lewis-conjugated glycopeptides from a proteolytic digestion of proteins. Furthermore, the protein sources of the Lewis-motif-conjugated glycopeptides could be identified by further MS^n of peptide-related ions.

In this study we demonstrated a method for the identification of Lewis x (Le^x, Galβ1−4(Fucα1−3)GlcNAc)-conjugated glycoproteins in tissue by LC−MS^n. Our method consists of two different runs of LC−MS^n using a Fourier-transform ion cyclotron resonance mass spectrometer (FTICR−MS) and ion trap-type mass spectrometer (IT-MS). After the first run, we sorted out the product ion spectra of expected Le^x-conjugated glycopeptides based on the presence of Lewis-motif-distinctive ions and assigned a peptide + HexNAc or peptide + (dHex-)HexNAc fragment in each spectrum. Then the fucosylated glycopeptides were subjected to a second run in which the peptide-related fragments were set as precursor ions (Figure 1). As a model tissue, we used a mouse kidney in which we previously confirmed the presence of the Galβ1−4(Fucα1−3)GlcNAc motif (Lewis x and y) as well as the absence of the Galβ1−3(Fucα1−4)GlcNAc motif (Lewis a and b) and Fucα1−2Galβ1−3/4GlcNAc motif (blood group H).[39]

Experimental Section

Materials. Trypsin (Trypsin Gold, mass spectrometry grade), *Aleuria aurantia* lectin (AAL)-immobilized agarose column and Peptide-*N*-glycosidase F (PNGase F) were purchased from Promega (Madison, WI), Honen (Tokyo, Japan) and Roche (Mannheim, Germany), respectively. Murine kidneys (MRL/MpJ-lpr/lpr) were purchased from Japan SLC Inc. (Hamamatsu, Japan).

Sample Preparation. Murine kidney cells were filtrated by a cell strainer (70 μm; BD Biosciences, San Jose, CA) and solubilized in lysis buffer (7 M urea, 2 M thiourea, 2% CHAPS, and 30 mM Tris-HCl) containing a protease inhibitor mixture (Wako, Tokyo, Japan) by vortexing at 4 °C. After quantifying the proteins, cold acetone (final concentration, 80%(v/v)) was added to the protein solution (500 μg protein). The precipitated protein was dissolved again in 100 μL of 0.5 M Tris-HCl, pH 7.0, and precipitated with an 8-fold volume of acetone. The precipitated protein was dissolved in 810 μL of 0.5 M Tris-HCl (pH 8.6) containing 8 M guanidine-HCl and 5 mM EDTA, and the mixture was incubated with 6.0 μL of 2-mercaptoethanol at room temperature for 2 h. Freshly prepared 0.6 M sodium monoiodoacetate (135 μL) was added to the solution, and the mixture was incubated at room temperature for 2 h in the dark. The reaction mixture was desalted with a PD10 column (GE Healthcare Bio-Sciences, Uppsala, Sweden), and the solution containing proteins was freeze-dried. The carboxymethylated proteins were dissolved in 500 μL of bicarbonate buffer (pH 8.5) and incubated with 2 μg of trypsin at 37 °C for 16 h. After deactivation of trypsin by boiling for 3 min, a 10-fold volume of phosphate buffered saline (PBS) was added to the reaction mixture.

Lectin Affinity Chromatography. The sample solution was applied to the AAL-immobilized agarose column (1.45 mg of lectin, 1.5 × 1.0 cm) and washed with 2.5 mL of cold PBS at 4 °C (approximately one drop/s). The absorbed glycopeptides were eluted with PBS containing 0.2 M fucose (2.5 mL), and the fraction was desalted with a C18 cartridge (Micro Trap, 8.0 × 1.0 mm; Michrom BioResources, Auburn, CA). The absorbed glycopeptides in the cartridge were eluted with 2 mL of 0.1% trifluoroacetic acid containing 45% acetonitrile, and the fraction was dried, resuspended in 0.1% formic acid, and then analyzed by LC−MS^n.

PNGase F Treatment. Fucosylated glycopeptides enriched by lectin affinity chromatography were treated with 10 units of PNGase F in 50 μL of 50 mM phosphate buffer (pH 8.0) at 37 °C for 48 h to release *N*-linked oligosaccharides. After terminating the reaction by boiling, the reaction mixture was evaporated to dryness, resuspended in 0.1% formic acid, and then analyzed by LC−MS/MS.

Online Liquid Chromatography/Mass Spectrometry (LC−MS). Chromatographic separation of the fucosylated glycopeptide was performed using the Paradigm MS4 HPLC system (Michrom BioResources). The fucosylated glycopeptides were dissolved in 25 μL of 0.1% formic acid, and 2 μL of the sample solution was injected into 2 μL capillary loop. The analytical column was a reversed-phase capillary column (Magic C18, 50 × 0.2 mm, 5 μm; Michrom BioResources). The mobile phase was 0.1% formic acid containing 2% acetonitrile (A buffer) and 0.1% formic acid containing 90% acetonitrile (B buffer). The fucosylated glycopeptides were eluted at a flow rate of 2 μL/min with a gradient of 5−65% of B buffer in 90 min.

Mass spectrometric analysis of fucosylated glycopeptides was performed using a FTICR/IT−MS (LTQ-FT; Thermo Fisher Scientific, Waltham, MA) equipped with a nanoelectrospray ion source (AMR, Tokyo, Japan). The conditions for FTICR−MS and IT−MS were as follows: an electrospray voltage of 2.0 kV in positive ion mode, a capillary temperature of 200 °C, a tube lens offset of 140 V, a collision energy of 35% for the MS^n experiment, maximum injection times (FTICR−MS and IT−MS) of 1250 and 50 ms, respectively, a resolution of FTICR−MS of 50 000, a scan time of approximately 0.2 s, dynamic exclusion of 18 s, and an isolation width of 3.0 u (range of precursor ion ±1.5).

First Run. The mass spectrometric mapping of fucosylated glycopeptides was performed by a sequential scan: full mass scan using FTICR−MS (*m/z* 1000−2000), data-dependent

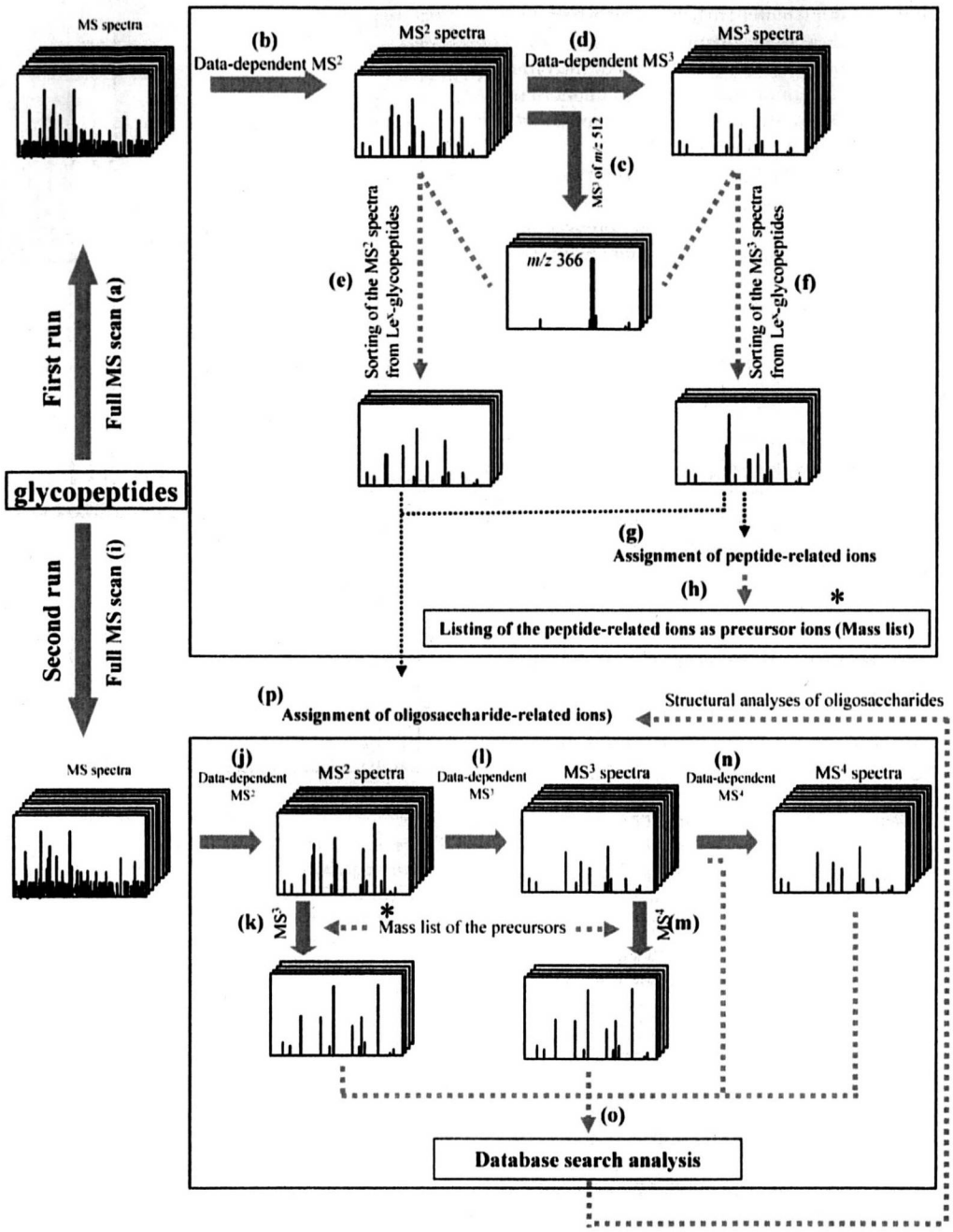

Figure 1. Strategy for the identification of Le^x-conjugated glycopeptides by LC−MS. The fucosylated glycopeptides were subjected to two different runs. In the first run, fucosylated glycopeptides were analyzed by (a) a full mass scan using the FTICR−MS, (b) data-dependent MS/MS, (c) MS/MS/MS of the Le^x-motif-distinctive ion (m/z 512), and (d) data-dependent MS/MS/MS. (e, f) On the basis of the presence of the product ion at m/z 512, which subsequently yielded the ion at m/z 366 by the MS/MS/MS, MS/MS and MS/MS/MS spectra of Le^x-conjugated glycopeptides were picked out from all the acquisition data. (g) Peptide-related ions were ascertained in the MS/MS/MS spectra. (h) The peptide-related ions were listed as precursor ions. In the second run, the fucosylated glycopeptides were identified by a full MS scan using the (i) FTICR-MS, (j) data-dependent MS/MS, (k) MS/MS/MS of the peptide-related ions listed as precursor ions, (l) data-dependent MS/MS/MS, (m) MS/MS/MS/MS of the peptide-related ions, and (n) data-dependent MS/MS/MS/MS. (o) Product ion spectra were submitted to database search analysis with a static modification of Cys with carboxymethyl (58.0 u) and possible modification of Asn with HexNAc (203.1 u) and dHex + HexNAc (349.1 u). MS^2, MS/MS; MS^3, MS/MS/MS; MS^4, MS/MS/MS/MS. (p) Carbohydrate structures were deduced from the oligosaccharide-related ions in the MS/MS and MS/MS/MS spectra.

MS/MS, MS/MS/MS of the Le^x-motif-distinctive ion (m/z 512) generated in data-dependent MS/MS, and MS/MS/MS of the most intense ions generated in data-dependent MS/MS by MS^n using IT−MS. Based on the presence of the product ion at m/z 512 that subsequently yielded the ion at m/z 366 by the MS/MS/MS, the MS/MS and MS/MS/MS spectra of expected Le^x-conjugated glycopeptides were picked out from all the acquisition data. Peptide-related ions were ascertained in the MS/MS/MS spectra, and were listed as precursor ions for the second run.

Second Run. Peptide sequencing was performed in a sequential scan: a full mass scan using FTICR–MS (*m/z* 1000–2000), data-dependent MS/MS, MS/MS/MS of the peptide-related ions listed as precursor ions, data-dependent MS/MS/MS, MS/MS/MS/MS of the peptide-related ions, and data-dependent MS/MS/MS/MS using IT–MS.

Protein Identification by Database Search Analysis. The spectra data obtained by the data-dependent collision-induced dissociation (CID)s and predominant CIDs of peptide-related ions were subjected to database search analysis with the TurboSEQUEST algorithm (BioWorks 3.1; Thermo Fisher Scientific) by using the NCBInr database (*Mus musculus*, 28–11–06). The static modification of carboxymethylation (58.0 u) at Cys, and the possible modification of HexNAc (203.1 u) and dHex + HexNAc (349.1 u) at Asn were used as the modified parameters of database search analysis. The SEQUEST criteria, known as cross correlation (Xcorr) scores, were set to 1.5/2.0/2.5 (charge states of +1/+2/+3) for the protein identifications. DTA files were generated for spectra with a threshold of 10 ions and a TIC of 100. Precursor and fragment ion mass tolerance in the MS^n spectra for database search analysis were set to 2.0 u and 1.0 u, respectively.

Results

Sorting out the Product Ion Spectra of the Le^x-Conjugated Glycopeptides by the First LC–MS/MS/MS Run. Proteins from mouse kidney cells were carboxymethylated and digested with trypsin. In the mass spectrometric mapping of the proteolytic digest, we often fail to acquire glycopeptide ions due to their lower ionization efficacy compared to coeluted unmodified peptides. To prevent interference by peptides in the ionization of glycopeptides, fucosylated glycopeptides including Lewis-motif-conjugated glycopeptides were enriched by affinity chromatography with an AAL-immobilized agarose column. The fucosylated glycopeptides were desalted by a C18 cartridge and injected into an LC–MS system equipped with FTICR–MS for a MS scan (*m/z* 1000–2000). The most intense ions on the MS scan were subjected to data-dependent MS/MS and MS/MS/MS, and an additional MS/MS/MS was performed when a dHex + Hex + HexNAc fragment (*m/z* 512) was detected on the MS/MS scan (Figure 1, first run). Figure 2A, B and C show the total ion chromatograms (TIC) obtained by the FTICR–MS scan of the fucosylated glycopeptides, the extracted ion chromatogram (EIC) of the dHex + Hex + HexNAc fragment acquired on the data-dependent MS/MS scan, and the EIC of the Hex + HexNAc fragment (*m/z* 366) that arose from the fragment at *m/z* 512 by the MS/MS/MS, respectively. We presumed that the Le^x-conjugated glycopeptides had been eluted around the peaks appearing in Figure 2C.

Assignments of the Peptide-Related Ions Derived from the Expected Le^x-Conjugated Glycopeptides. We picked out dozens of product ion spectra, and 22 precursors were determined to be the Le^x-conjugated glycopeptide-derived mass spectra based on the presence of Le^x-motif-distinctive ions. The elution positions of the glycopeptides are indicated in Figure 2C. In our previous report, most of the *N*-glycosylated peptides yielded peptide-related ions, such as $[peptide + HexNAc + nH]^{n+}$ and $[peptide + (dHex)HexNAc + nH]^{n+}$, which provided peptide fragment b- and y-ions by further CID, and subsequent database search analysis successfully revealed the peptide sequences of the glycopeptides.[27] In the present study, therefore, we examined the peptide-related ions in the product ion spectra of the glycopeptides 1–22 for peptide sequencing.

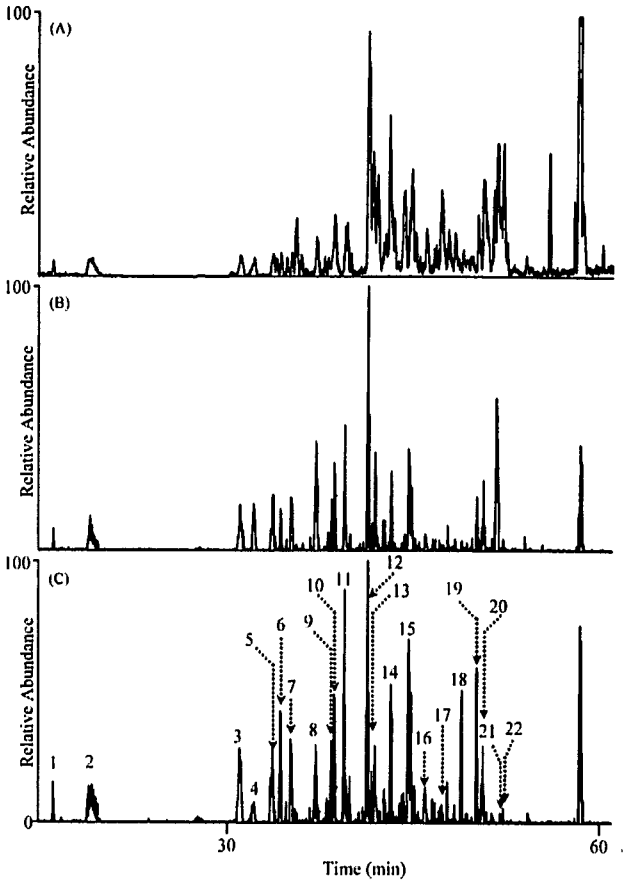

Figure 2. LC–MS^n of fucosylated glycopeptides. (A) Total ion chromatogram (TIC, *m/z* 1000–2000) of fucosylated glycopeptides. (B) Extracted ion chromatogram (EIC) of the ion at *m/z* 512 produced by data-dependent MS/MS. (C) EIC of the product ions at *m/z* 366 produced from the product ion at *m/z* 512 by MS/MS/MS. Expected Le^x-conjugated glycopeptides were designated as glycopeptides 1–22.

Figure 3A shows the integrated mass spectrum of the expected Le^x-glycopeptides eluted at 41–43 min. On the basis of an *m/z* spacing pattern that included *m/z* 67.69 ($HexNAc^{3+}$), *m/z* 54.02 (Hex^{3+}) and 48.69 ($dHex^{3+}$), intense ions at *m/z* 1067.105, 1134.803, 1189.505, and 1237.508 were assigned to triply charged ions of glycopeptides differing in glycosylation. Two intense ions, glycopeptides 12 (*m/z* 1237.508) and 13 (*m/z* 1134.803), were further subjected to MS/MS and MS/MS/MS, and yielded identical peptide-related ions at *m/z* 1650 (Figure 3B, C). This result indicates that glycopeptides 12 and 13 are glycoforms containing Le^x-motifs, and implies that the carbohydrate heterogeneity of a peptide of interest could be deduced from the integrated mass spectra.

Figure 4A indicates the MS/MS spectrum of glycopeptide 8. The presence of a dHex + Hex + HexNAc fragment (*m/z* 512) suggests that this glycopeptide is one of the Le^x-conjugated glycopeptides. The most intense fragment (*m/z* 1681.0) was further subjected to MS/MS/MS and provided a series of doubly charged Y-ions with an *m/z* spacing pattern, including *m/z* 101 ($HexNAc^{2+}$) and *m/z* 81 (Hex^{2+}). It was revealed that the fragment at *m/z* 906.2 was our desired product ion, $[peptide + HexNAc + 2H]^{2+}$ (Figure 4B).

Figure 5A and B show the MS/MS and MS/MS/MS spectra of glycopeptide 15, respectively. The triply charged ion (*m/z* 1414.4)

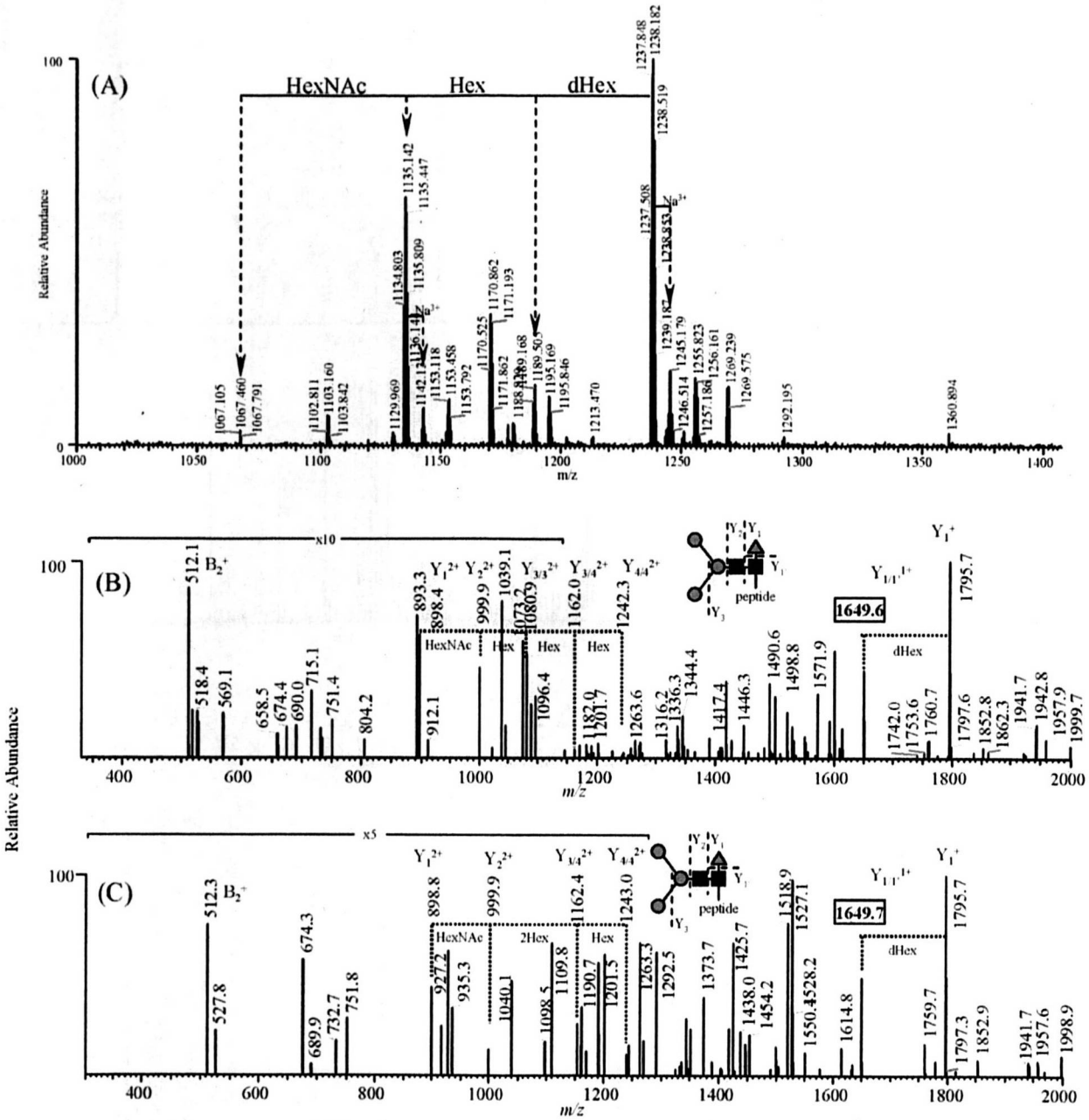

Figure 3. Integrated mass spectrum and MS/MS/MS spectra of glycopeptides 12 and 13. (A) Integrated mass spectrum of the expected Le^x-glycopeptides eluted at 41−43 min. (B) MS/MS/MS spectrum acquired from the most intense ion (*m/z* 1673.4) detected in the MS/MS spectrum of glycopeptide 12 (*m/z* 1237.8). (C) MS/MS/MS spectrum acquired from the most intense ion (*m/z* 1601.0) detected in the MS/MS spectrum of glycopeptide 13 (*m/z* 1135.4).

on the MS/MS scan was further subjected to MS/MS/MS and yielded a Y-ion series that included [peptide + 2HexNAc + 3Hex + dHex + 2H]$^{2+}$ (*m/z* 1764.3), [peptide + 2HexNAc + 2Hex + dHex+ 2H]$^{2+}$ (*m/z* 1683.5), [peptide + 2HexNAc + dHex + 2H]$^{2+}$ (*m/z* 1520.2), and [peptide + 2HexNAc + 2H]$^{2+}$ (*m/z* 1447.0). The fragment detected at *m/z* 1346.3 was assigned to our target ion, [peptide + HexNAc + 2H]$^{2+}$.

Alternative MS/MS and MS/MS/MS spectra of a Le^x-conjugated glycopeptide (glycopeptide 17) are shown in Figure 6A and B, respectively. The fragment at *m/z* 1515.4 on the MS/MS scan yielded Y-ion series that included [peptide + 2HexNAc + 3Hex + 2H]$^{2+}$ (*m/z* 1659.6), [peptide + 2HexNAc + 2Hex + 2H]$^{2+}$ (*m/z* 1578.3), and [peptide + 2HexNAc + 2H]$^{2+}$ (*m/z* 1416.5) on the MS/MS/MS scan. We deduced that the fragment at 1315.0 on the MS/MS/MS scan could be [peptide + HexNAc + 2H]$^{2+}$.

Finally we assigned out peptide + HexNAc, peptide + (dHex)HexNAc, and the peptide fragment from the product ion spectra of Le^x-conjugated glycopeptides 1−22 (Table 1). These peptide-related ions were listed as precursor ions in the second run, in which the listed ions were predominantly submitted to CID (Figure 1, second run).

Peptide Sequencing of the Expected Le^x-Conjugated Glycopeptides by the Second LC−MS/MS/MS/MS Run and Database Search Analysis. In the second run and subsequent database search analysis with modified parameters, including

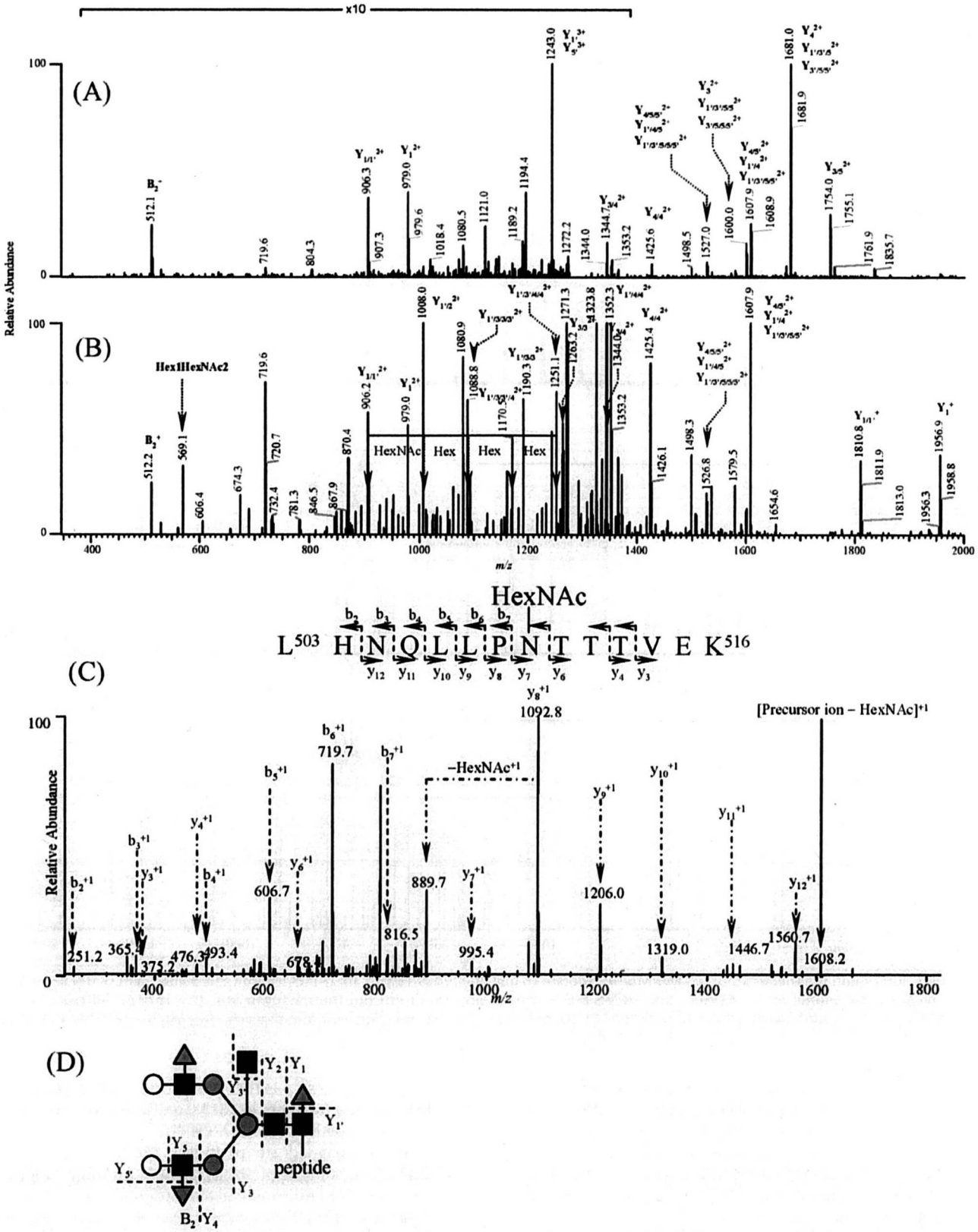

Figure 4. Identification of glycopeptide 8. (A) MS/MS spectrum acquired from the molecular ion $[M + 3H]^{3+}$ (*m/z* 1291.9) of glycopeptide 8 in Figure 2A. (B) MS/MS/MS spectrum acquired from the most intense ion (*m/z* 1681.0) in the MS/MS. (C) MS/MS/MS/MS spectrum acquired from the product ion (*m/z* 906.2) in the MS/MS/MS of glycopeptide 8, and amino acid sequence deduced from the results of database search analysis. (D) Deduced oligosaccharide structure. dHex, deoxyhexose; Hex, hexose; HexNAc, *N*-acetylhexosamine: white circle, galactose; gray circle, mannose; black square, *N*-acetylglucosamine; gray triangle, fucose.